nature cancer

ARTICLES

https://doi.org/10.1038/s43018-021-00207-7

Clonal expansion of T memory stem cells determines early anti-leukemic responses and long-term CAR T cell persistence in patients

Luca Biasco[1,2], Natalia Izotova[1], Christine Rivat[1], Sara Ghorashian[3], Rachel Richardson[1], Aleks Guvenel[1], Rachael Hough[4], Robert Wynn[5], Bilyana Popova[6], Andre Lopes[6], Martin Pule[7], Adrian J. Thrasher[1] and Persis J. Amrolia[1,8]✉

Low-affinity CD19 chimeric antigen receptor (CAR) T cells display enhanced expansion and persistence, enabling fate tracking through integration site analysis. Here we show that integration sites from early (1 month) and late (>3 yr) timepoints cluster separately, suggesting different clonal contribution to early responses and prolonged anti-leukemic surveillance. CAR T central and effector memory cells in patients with long-term persistence remained highly polyclonal, whereas diversity dropped rapidly in patients with limited CAR T persistence. Analysis of shared integrants between the CAR T cell product and post-infusion demonstrated that, despite their low frequency, T memory stem cell clones in the product contributed substantially to the circulating CAR T cell pools, during both early expansion and long-term persistence. Our data may help identify patients at risk of early loss of CAR T cells and highlight the critical role of T memory stem cells both in mediating early anti-leukemic responses and in long-term surveillance by CAR T cells.

Adoptive T cell transfer shows great promise for the treatment of both viral infections and cancer but much remains to be learnt about the optimal phenotype of T cell products, their clonal dynamics once infused and the origin of both early responding T cells that mediate initial responses as well as long-term-persisting T cells that provide immunological surveillance. According to the hierarchical model of T cell differentiation, upon antigenic priming naïve T (T_N) cells differentiate into central memory (T_{CM}) cells that express lymph node homing molecules but have limited effector function, which in turn give rise to effector memory (T_{EM}) cells that preferentially traffic to the tissues and differentiate to terminally differentiated effector cells (T effector memory CD45RA$^+$ (T_{EMRA}) cells) that mediate rapid effector functions[1]. Subsequently, Gattinoni et al.[2] demonstrated the existence of the stem cell memory (T_{SCM}) compartment, with a naïve surface phenotype and high proliferative capacity but also attributes of memory T cells, which appears endowed with both the potential for multipotent differentiation and long-term self-renewal. For durable anti-viral/anti-tumor responses long-term immune surveillance is critical, but the ontogeny of T cells mediating such long-term responses remains a matter of active debate. Early data from adoptive transfer of gene-marked Epstein-Barr virus (EBV)-specific T cells, which had a predominantly T_{EM} phenotype at infusion, showed these could be detected up to 9 yr post-infusion[3]. In a macaque model, cytomegalovirus (CMV)-specific CD8 T cell clones derived from T_{CM} (but not T_{EM}) cells persisted long term after adoptive transfer[4]. Tracking of T cells retrovirally transduced to express adenosine deaminase (ADA) using integration site (IS) analysis has demonstrated that genetically engineered T_{SCM} clones persist and preserve their differentiation potential for up to 12 yr post-infusion[5]. On the other hand, similar analyses of marked circulating T cells 2–14 yr after infusion of T cells retrovirally transduced with the herpes simplex virus (HSV) thymidine kinase suicide gene suggested that long-term-persisting marked cells arose predominantly from both infused T_{SCM} and T_{CM} compartments[6].

CD19 CAR T cells show unprecedented responses in relapsed/refractory acute lymphoblastic leukemia (ALL)[7–10]. Anti-leukemic responses correlate with both the level of early CAR T cell expansion[11] and the duration of CAR T cell engraftment, with long-term persistence critical for durable remission if used as a stand-alone therapy. The origins of early expanding and long-term-persisting CAR T cells may differ and have yet to be defined. This will be critical in designing manufacturing protocols to optimize outcomes. Initial data in a xenogeneic mouse model of mesothelioma where mesothelin CAR-transduced human CD8$^+$ T_{SCM}/T_{CM}/T_{EM} cells were infused with CD4$^+$ CAR T cells demonstrated superior anti-tumor responses with T_{SCM}[2]. In a xenogeneic model of lymphoma, CD19 CAR T cells derived from selected CD4$^+$ T_N and CD8$^+$ T_{CM} populations gave superior anti-tumor activity, and a 1:1 combination of bulk CD4$^+$ and CD8$^+$ T_{CM} CD19 CAR T cells showed optimal activity[12], leading the investigators to test this approach clinically in adult ALL[13]. Xu et al.[14] found that the expansion of CD19 CAR T cells in patients correlated with the frequency of CD8$^+$CD45RA$^+$CCR7$^+$ within the infused product whose phenotype approximated T_{SCM} (it should be noted that in this study T_N cells were not distinguished from T_{SCM} by evaluation of CD95 expression), although CAR T cell

[1]Molecular and Cellular Immunology Section, UCL Great Ormond Street Institute of Child Health, London, UK. [2]Gene Therapy Program, Dana-Farber/Boston Children's Cancer and Blood Disorders Center, Harvard Medical School, Boston, MA, USA. [3]Molecular Haematology Section, UCL Great Ormond Street Institute of Child Health, London, UK. [4]Department of Haematology, University College London Hospital, London, UK. [5]Department of Bone Marrow Transplant, Royal Manchester Children's Hospital, Manchester, UK. [6]CRUK UCL Cancer Trials Centre, University College London, London, UK. [7]University College London Cancer Institute, London, UK. [8]Department of Bone Marrow Transplantation, Great Ormond Street Hospital, London, UK. ✉e-mail: Persis.Amrolia@gosh.nhs.uk

expansion and persistence in this study were poor, possibly due to the lack of lymphodepletion and the use of a CD28 costimulatory domain, respectively. Little is known about the how the phenotype and clonal composition of CAR T cells change following adoptive transfer. IS analysis offers us a unique tool to track the clonal dynamics of genetically modified CAR T cells in patients, as each transduced cell is stably marked by a vector IS acting as a genetic barcode. Using T cell receptor (TCR)-β and IS analysis, Sheih et al.[15] have shown that CAR T cells at early timepoints post-infusion are polyclonal but that individual clones display different clonal kinetics after infusion. However, because of limited CAR T cell persistence in this study, the analysis was restricted to 30 d post-infusion. Moreover, it is not clear whether these data are skewed by the use of the infused products derived from selected $CD4^+$ and $CD8^+$ T_{CM} cells. To date, it has not been possible to isolate long-term (>1 yr) persisting CAR T cells in patients. In the immunotherapy with CD19 CAR T cells for high-risk relapsed/refractory pediatric $CD19^+$ acute lymphoblastic leukemia (CARPALL) phase 1 study, the use of an improved low-affinity CD19 CAR resulted in enhanced expansion and persistence of CAR T cells post-infusion[16], enabling us for the first time, to our knowledge, to detect and select long-term-persisting CAR T cell flow cytometrically. By combining phenotypic analysis after treatment with high-resolution IS analysis of selected CAR T cells, we have analyzed the fate of infused CAR T cells in two patients with long-term persistent CAR T cells in peripheral blood and compared this with two patients who had early loss of CAR T cells (Fig. 1a).

Results

CAR T cell kinetics and phenotype post-infusion. To study the composition of CAR T cells in our patients over time, we performed a comprehensive immunophenotypic analysis for the detection of CAR cells and for the characterization of different T cell subtypes (Fig. 1b,c). All four patients analyzed showed similar kinetics of CAR T cell engraftment, showing relative contribution in the $CD3^+$ compartment as high as 14–80% at the time of peak expansion (day 14) followed by contraction to 6–30% by day 30 (reflecting elimination of $CD19^+$ targets), and then low-level long-term persistence in patient 4 (Pt4) and Pt6 (0.1% at 36 and 28 months) (Fig. 1d,e). We then assessed the naïve/memory phenotype of CAR T cells in both the infused product and the peripheral blood post-infusion flow cytometrically, using CD45RA, CD62L and CD95 as markers (Extended Data Fig. 1). In the patients with long-term CAR T cell persistence, the infused CAR T cell product was primarily composed of T_{CM} (78–81% of CAR^+ T cells) with a lower contribution of T_{EM} (17–21%), but also a small but detectable pool (1–2%) of T_{SCM} (Fig. 1f). Following infusion, in both of these patients the composition of CAR T cells switched substantially towards the T_{EM} phenotype, which became the predominant fraction at both early and late timepoints (Fig. 2e). There was a small increase in the percentage of terminally differentiated effector CAR T cells (T_{EMRA} cells) in both patients up to the 6-month timepoint, but this declined thereafter. Interestingly, the small fraction of T_{SCM} cells present upon infusion became increasingly represented over time, implying that the CAR T_{SCM} cells detected in the cell product are indeed endowed with high self-renewing potential after infusion.

For comparison, we performed a similar phenotyping analysis on CAR T cells from two patients (Pt10 and Pt17) who lost circulating CAR T cells at 2- and 4-months post-infusion to investigate whether differences in product composition or relative engraftment of T cell subsets might correlate with lack of persistence in patients. As shown in Fig. 2, the CAR T cell products (particularly in Pt17) had a more differentiated phenotype with a lower proportion of T_{SCM} and higher T_{EM} than in the patients with long-term persistence (Fig. 2a,b,d). Similarly, by day 30 post-infusion, CAR T cells from these patients showed a predominantly T_{EM} phenotype, whereas in Pt4 and Pt6 we observed a substantially higher preservation of the T_{SCM} and T_{CM} compartments (Fig. 2a,c).

IS analysis of CAR T cells. Next, we characterized CAR T cells of these patients at the single-clone level to address the following questions: (1) What are the CAR T cell clonal dynamics occurring during the acute anti-tumor response phase versus steady state? (2) What is the clonal composition of the long-surviving CAR T cells? And, (3) which fraction of the cell product contributes the most to the long-term maintenance of CAR cells in these patients? To this aim, we collected, through our well-established protocol that combines FACS of blood cell subpopulations, whole-genome amplification, linear amplification-mediated PCR and high-throughput sequencing (Illumina)[5], a total of 9,881 and 3,667 ISs from T_{SCM}, T_{CM} and T_{EM} isolated from the cell products of Pt4 and Pt6, respectively. Similarly, we were also able to collect 4,417 and 6,646 ISs in Pt4 and Pt6, respectively, from FACS-sorted CAR T_{SCM} and T_{CM}/T_{EM} cells at 14 and 30 d after infusion, as well as 1,676 and 1,930 unique ISs from the total circulating CAR cells of both individuals, respectively, at 180 and 720/840 d after treatment (Extended Data Fig. 2). It should be noted that it was not possible to select subpopulations at these later timepoints due to the low fraction of CAR cells in circulation. The number of ISs collected at long-term follow-ups is well above that previously reported at similar timepoints after CAR T cell treatment[17], and suggests that while clonal diversity decreases somewhat post-infusion, CAR T cells remain highly polyclonal even at late timepoints post-infusion. We then analyzed the distribution of our ISs in the genomes of CAR T cells from the infused products and isolated post-infusion at both early and late timepoints. As shown in Fig. 3 (top panels) and Extended Data Fig. 3, in the cell products the lentiviral vector integrated into (on average 69% of ISs in both patients) or in proximity to a variety of different genes, most of which are classical targets of lentiviral integrations in gene therapy[18], with a prevalence of genes related to biological processes such as DNA metabolism and repair (Extended Data Fig. 4). Notably, there was no evidence of clonal selection after infusion with respect with the general insertional profile (Fig. 3, bottom panels, and Extended Data Fig. 3), or of clones with lentiviral genomic insertions in proximity to genes exerting a specific cellular function (Extended Data Fig. 4).

Fig. 1 | Immunophenotypic characterization of patients with long-lasting CAR T cells in the product and after infusion over time. a, Schematic summarizing the manufacture of CAR T cells and key aspects of CARPALL clinical study design. The days reported in this schematic are reflective of the days of in vitro expansion since PBMC isolation. **b**, Schematic representation of survival and expansion potential of the main T cell subpopulations. **c**, Gating scheme used for the identification of T cell subtypes used for following up CAR T cells and total $CD3^+$ cells. **d**, FACS plot showing CAR cells within $CD3^+$ cells as well as T cell composition inside the CAR^+CD3^+ $CD45RA^+CD62L^+$ population for Pt4 (top panels) and Pt6 (bottom panels). Percentages of CAR cells and CD62L/CD45RA compartments are showed inside each gate. Timepoints of analysis are shown on top of each set of panels (d, days after CAR cell infusion). **e**, Percentage of CAR cells in the $CD3^+$ cell compartment over time in Pt4 (top panel) and Pt6 (bottom panel). **f**, Summary of data shown in panel **c** for CAR T cell composition over time for Pt4 (left panel) and Pt6 (right panel). Pie charts show composition of CAR T cells at each timepoint. Longitudinal contribution of each subpopulation to the CAR cell compartment is shown in the relative plot below. aCD3, anti-CD3; aCD28, anti-CD28; CAT, CAR molecule CAT-19; FSC-A, forward scatter; SSC-A, side scatter.

Clonal diversity is preserved in long-lasting CAR T cells. We next assessed the diversity of CAR T cells in the CAR T products by means of number and relative contribution of ISs collected starting from FACS-sorted T_{SCM}, T_{CM} or T_{EM} cells. Because the frequency of these populations differed in the cell product, to normalize for this we used equal amounts of genomic DNA from each subpopulation

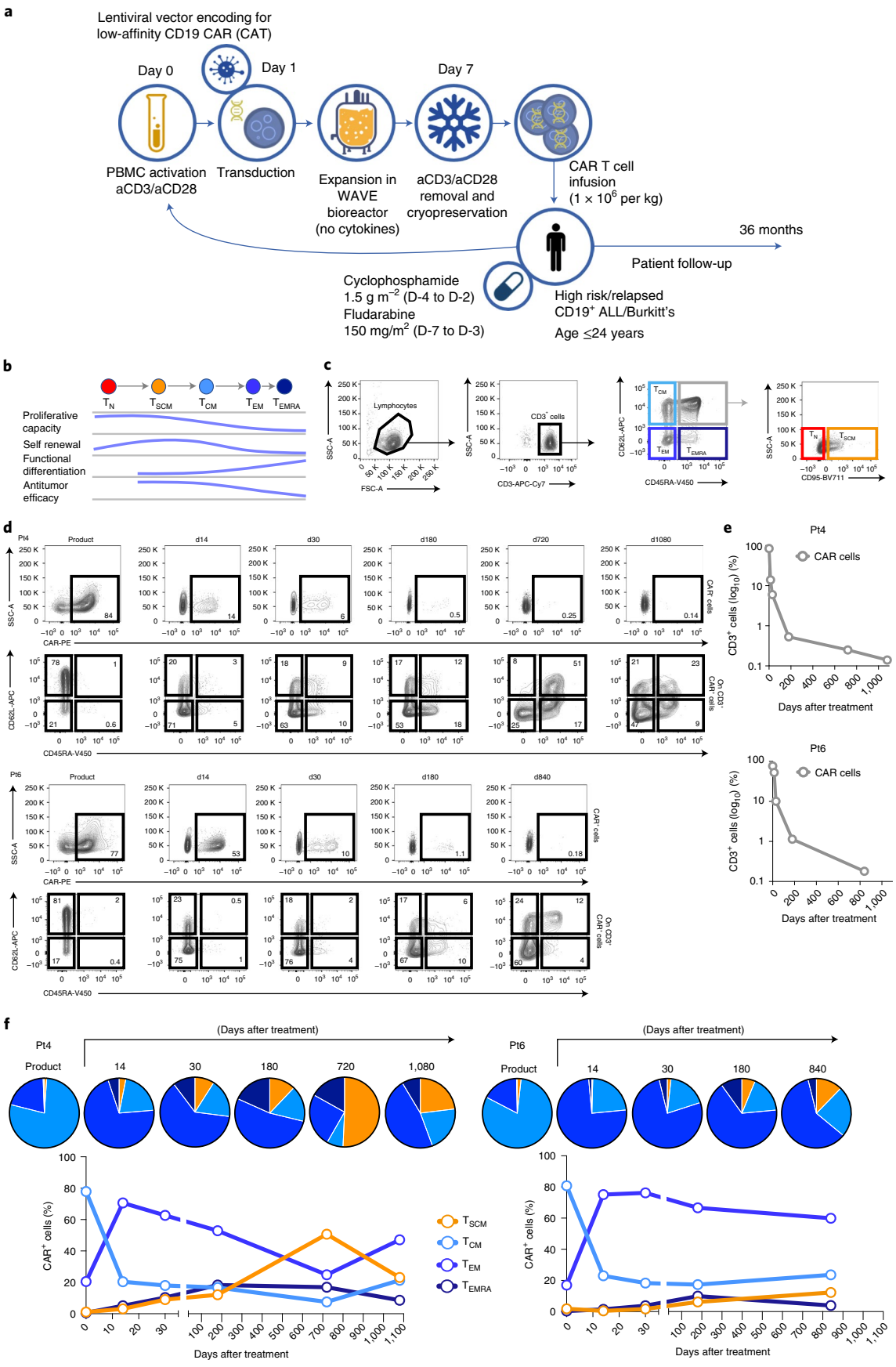

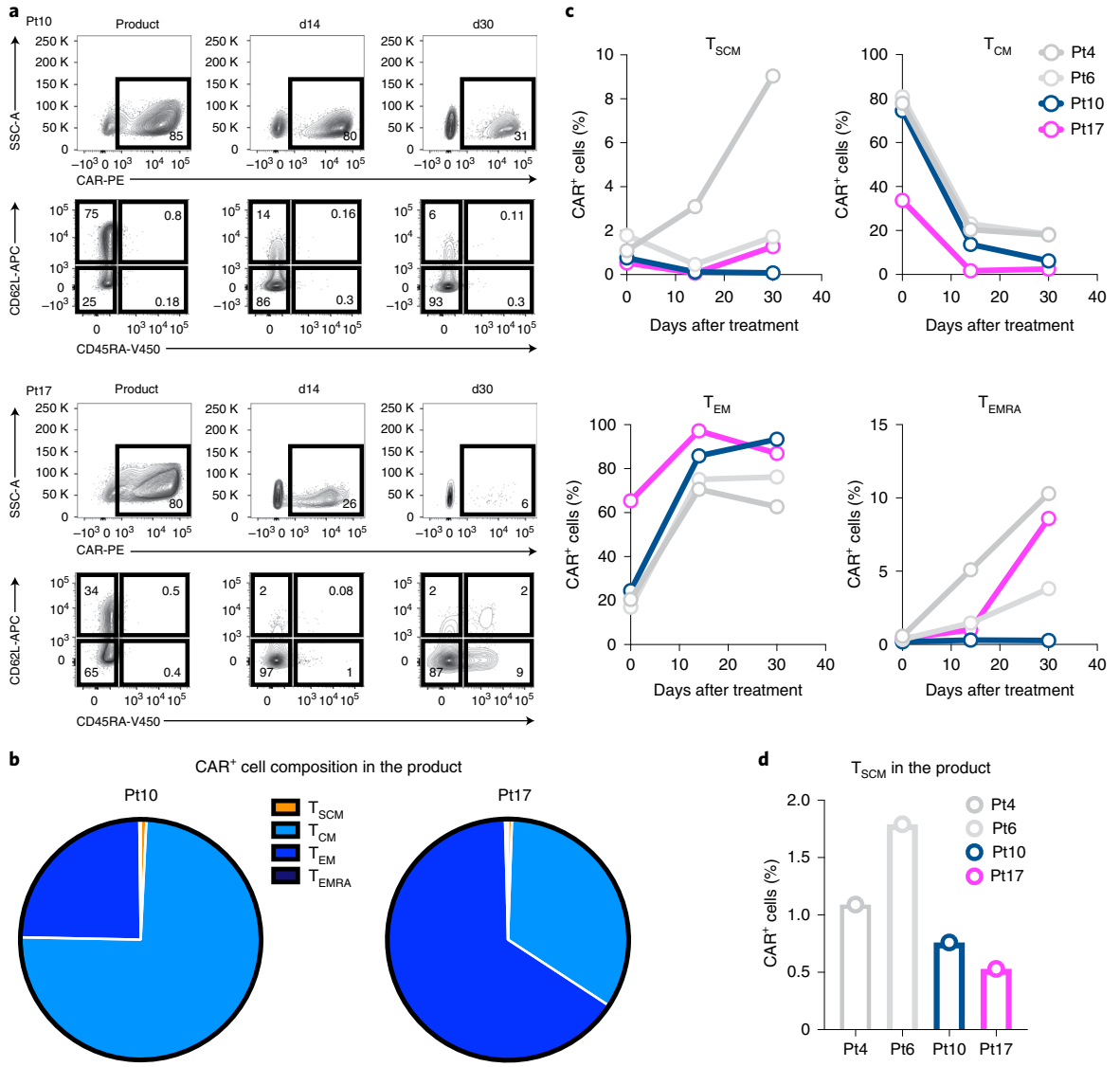

Fig. 2 | Immunophenotypic characterization of patients with short-living CAR T cells in the product and after infusion over time. a, FACS plot showing CAR cells within CD3+ cells as well as T cell composition inside the CARCD3+CD45RA+CD62L+ population for Pt10 (top panels) and Pt17 (bottom panels). Percentages of CAR cells and CD62L/CD45RA compartments are shown inside each gate. Timepoints of analysis are shown on top of each set of panels (d, days after CAR cells infusion). **b**, Pie charts showing the composition of the drug product in Pt10 and Pt17. **c**, Longitudinal contribution of each subpopulation to the CAR cell compartment in Pt10 and Pt17 versus Pt4 and Pt6. **d**, Bar plot showing the relative fraction of T_{SCM} cells detected in the drug product in Pt4 and Pt6 versus Pt10 and Pt17.

for performing IS analysis. All subpopulations showed high diversity in both patients 4 and 6, with the biggest clones ranging from 2.1% to 14.7% of each population (with the exception of one clone with ISs contributing to 30.4% of the reads collected from the T_{EM} of Pt6) (Figs. 4 and 5, top panels, and Extended Data Fig. 5a). Of note, the T_{CM} fraction of both individuals showed a higher number of integrants and higher diversity as compared with the other two populations. This suggests that T_{CM} may be more permissive to transduction as compared with T_{SCM} and T_{EM}, possibly as a result of a higher activation/expansion during in vitro transduction. Based on our initial observation on the increasing relative contribution of T_{SCM} in circulation as compared with that infused in the cell product, we investigated the clonal dynamics of this population after infusion in more detail. To do this, we isolated the T_{SCM} from the rest of the memory/effector cell fractions in the early response phase (14 and 30 d post-infusion) when the number of circulating CAR cells in circulation permitted cell sorting of CAR T cell subfractions. In Figs. 4 and 5 (bottom panels), we compared the IS profile of sorted CAR T_{SCM} cells with the rest of the CAR population at the same timepoints. We observed that in both patients the clonal diversity of T_{SCM} (measured either as Shannon or as Gini–Simpson diversity and shown in Figs. 4 and 5, bottom panels, and Extended Data Fig. 5d, respectively) dropped substantially during the early response phase compared with the infused product. Most of the T_{SCM} cells isolated from patients early after treatment were in fact composed of individual clones bearing ISs whose reads ranged from 89.0% to 96.9% of the total read count (Extended Data Fig. 5b). It is important to note that neither the number of sorted cells nor the amount of ISs collected per sample would alone explain this finding (Extended Data Fig. 6), and that the same experimental conditions have been applied to the study of small subfractions of progenitor cells in gene therapy patients with different results[19]. This observation is instead

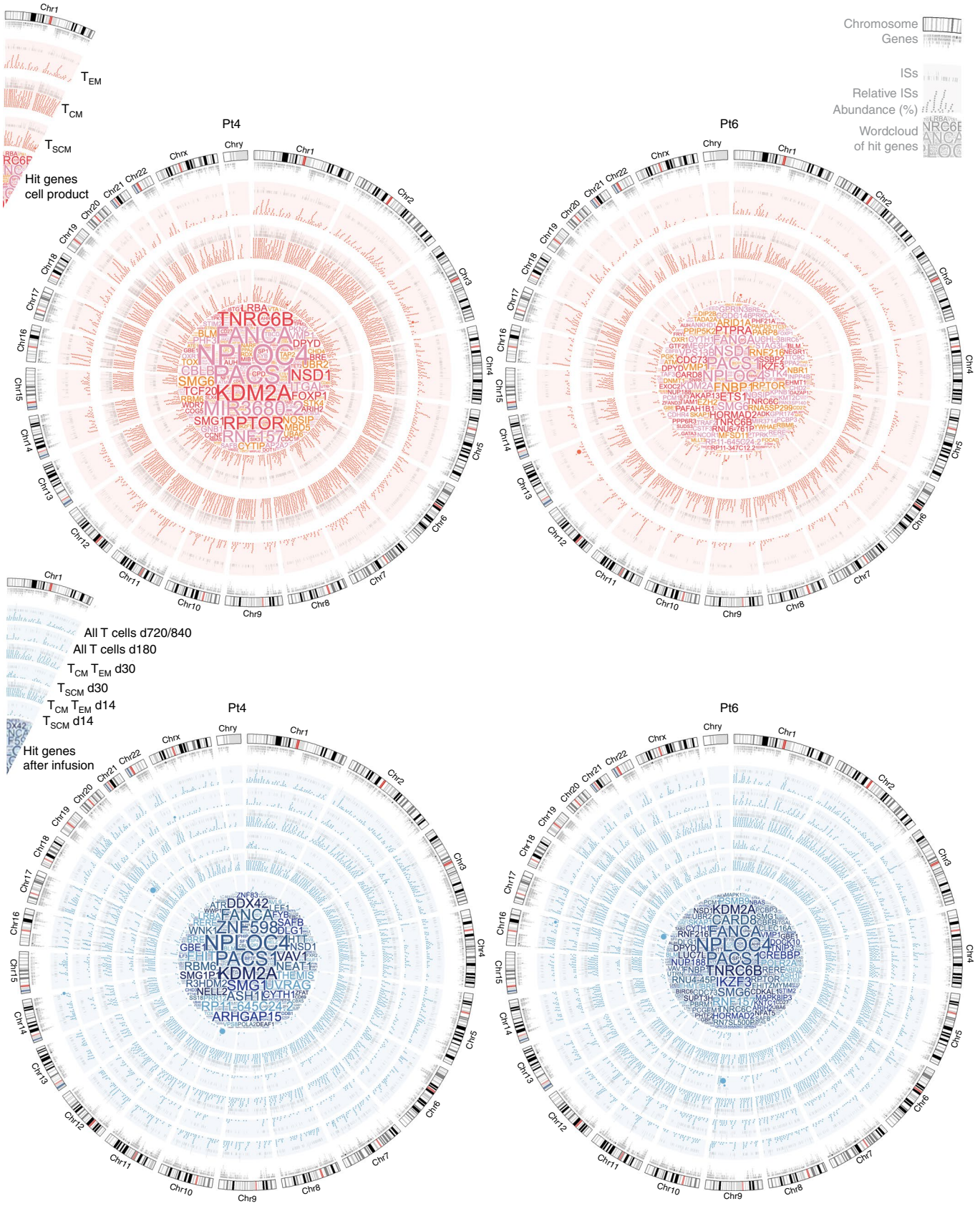

Fig. 3 | Distribution and abundance of ISs collected in the product and after infusion over time in Pt4 and Pt6. Circos plot showing the genomic distribution of ISs in the product (top panels) and after infusion (bottom panels) in Pt4 (left panels) and Pt6 (right panels). Descriptions of each concentric data track and timepoint (d, days after CAR cells infusion) are shown in the legends on the left of the circus plots. Descriptions of the contents of these plots are reported in the gray legend on the top right. Word clouds showing top hit genes in the product and after infusion are shown at the center of each plot (the bigger the gene name the higher the number of ISs detected in its locus). Chr, chromosome.

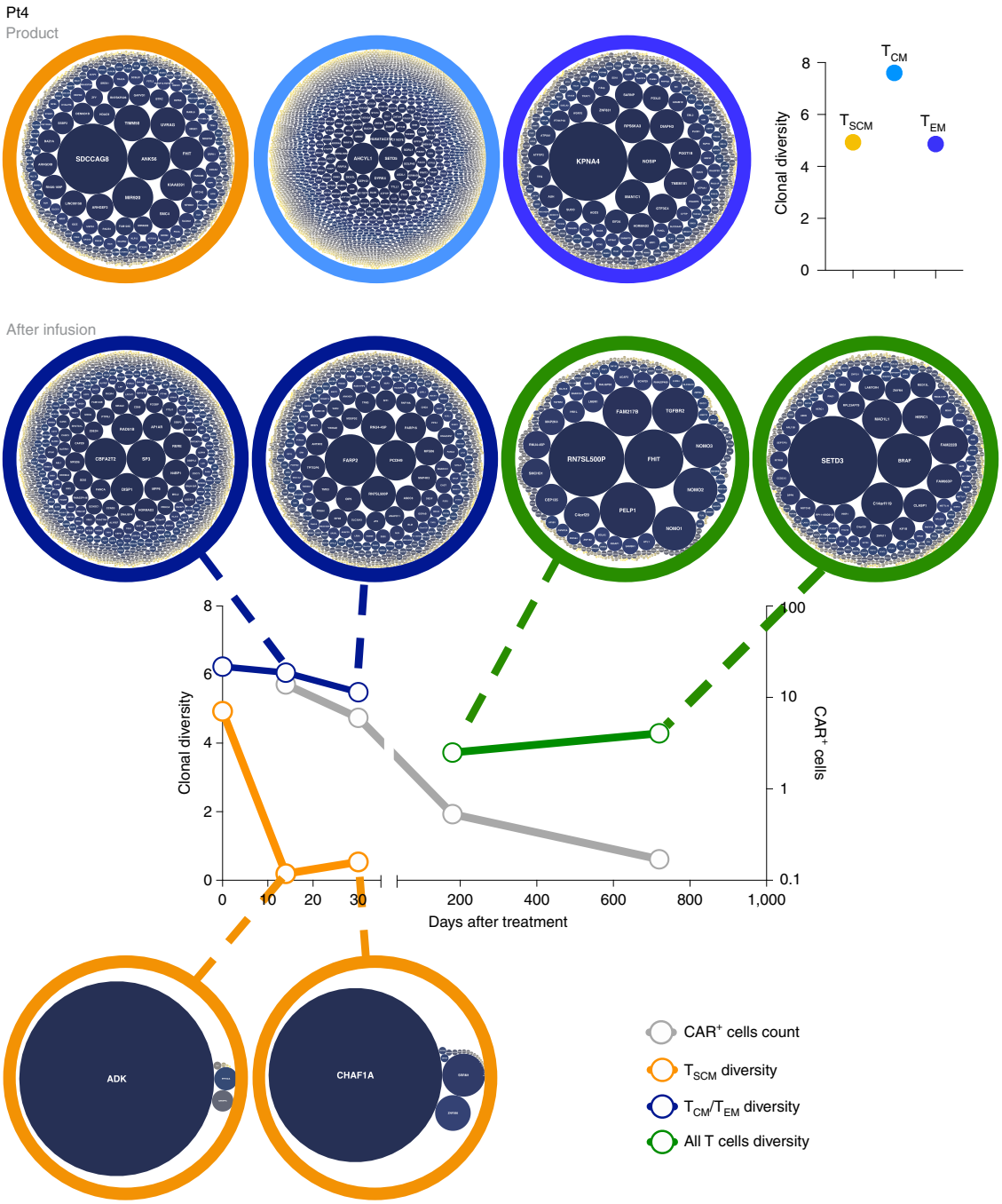

Fig. 4 | Diversity of ISs in different T cell subtypes over time from Pt4. Top panels, for each product subpopulation analyzed, colored circles (T_{SCM}, orange; T_{CM}, light blue; T_{EM}, blue) contain bubble plots of clones contributing >0.01% to the total population. The dimension of the bubble is proportional to the size of the clone. The name of the gene closest to the relative IS is reported inside the bubble. The plots on the right show Shannon diversity index for each subpopulation. Bottom panels, plots showing Shannon diversity index (left *y* axis) of ISs over time in T_{SCM} cells (orange lines) and in T_{CM}/T_{EM} cells (dark blue) and in all T cells (green lines). The gray lines show the percentage of CAR cells over time (right *y* axis). For each timepoint analyzed, colored circles contain bubble plots of clones contributing >0.01% to the total population at each timepoint. The dimension of the bubble is proportional to the size of the clone. The name of the gene closest to the relative IS is reported inside each bubble.

likely a reflection of bona fide clonal bursts and oligoclonal expansion occurring in T_{SCM} cells during the early response phase (Figs. 4 and 5, bottom panels). At the same timepoints, the clonal composition of the remaining CAR cells (T_{CM}/T_{EM}) remained highly polyclonal despite the major shift from T_{CM} to T_{EM} phenotype occurring upon infusion, as described above. This would suggest that the CAR T_{CM} and T_{EM} cells infused in these patients have expanded in a more 'homeostatic' fashion as compared with their T_{SCM} counterparts.

We then analyzed in both patients the diversity of the total CAR cell composition at later timepoints (180 and 720/840 d after infusion). While the frequency of CAR cells dropped substantially from the initial phase, we observed that the clonal diversity of long-term-persisting CAR T cells remained high (Figs. 4 and 5, bottom panels, and Extended Data Fig. 5c). This suggests that CAR T cells detected at late timepoints have persisted through 'homeostatic' survival and that long-term maintenance of CAR cells in our

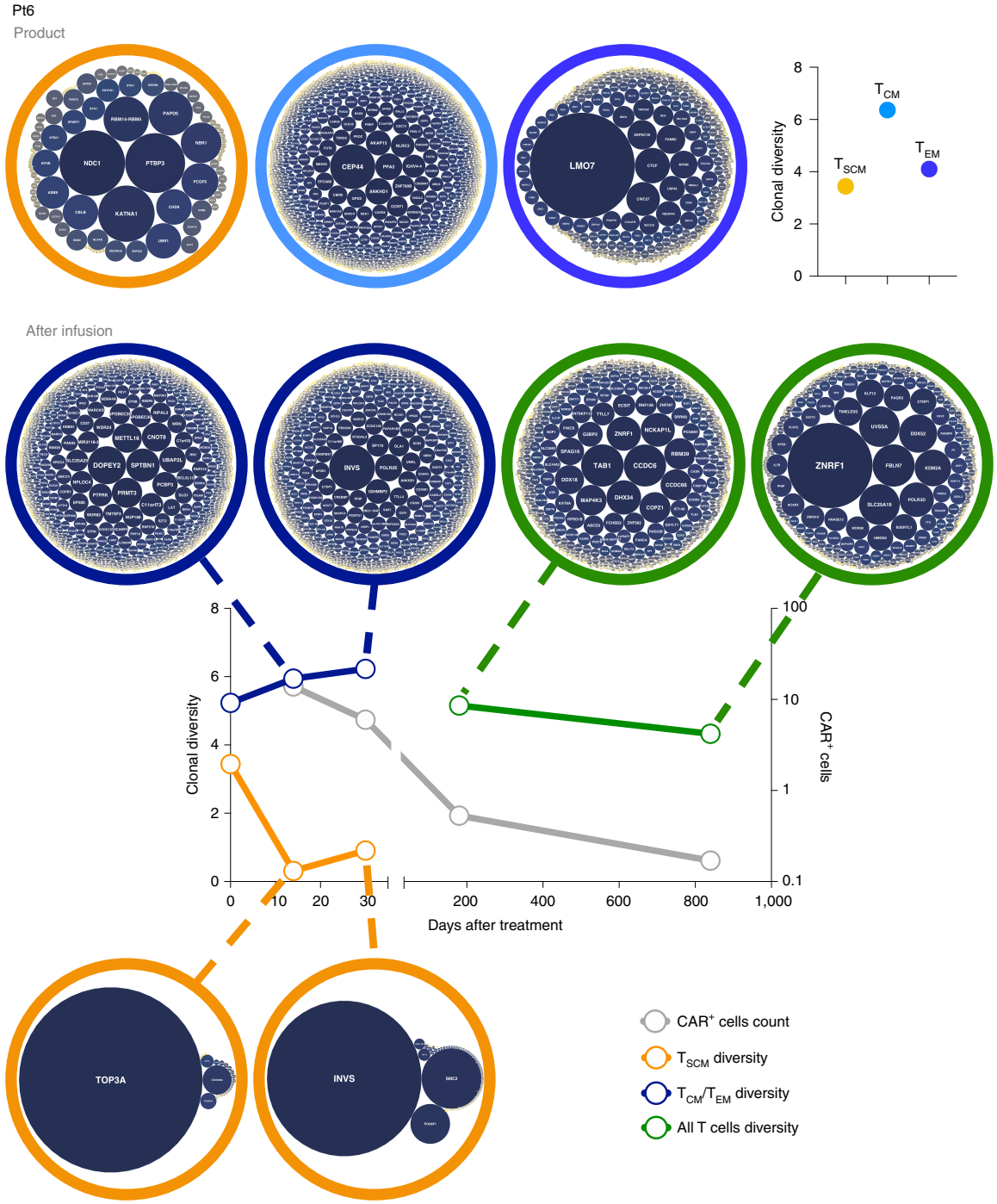

Fig. 5 | Diversity of ISs in different T cell subtypes over time from Pt6. Top panels, for each product subpopulation analyzed, colored circles (T_{SCM}, orange; T_{CM}, light blue; T_{EM}, blue) contain bubble plots of clones contributing >0.01% to the total population. The dimension of the bubble is proportional to the size of the clone. The name of the gene closest to the relative IS is reported inside the bubble. The plots on the right show Shannon diversity index for each subpopulation. Bottom panels, plots showing Shannon diversity index (left *y* axis) of ISs over time in T_{SCM} cells (orange lines) and in T_{CM}/T_{EM} cells (dark blue) and in all T cells (green lines). The gray lines show the percentage of CAR cells over time (right *y* axis). For each timepoint analyzed, colored circles contain bubble plots of clones contributing >0.01% to the total population at each timepoint. The dimension of the bubble is proportional to the size of the clone. The name of the gene closest to the relative IS is reported inside each bubble. Analysis performed as in Fig. 4.

patients was not dependent on the expansion of a few large clones carrying nonphysiological/aberrant insertional profiles.

To study the clonal dynamics of CAR T cells over time, we first compared all datasets from early or late timepoints and performed unsupervised clustering according to IS similarities (Fig. 6a). We found that ISs isolated at 14 and 30 d after infusion showed the highest similarities and clustered separately from the clonal datasets of 180 and 720/840 d, suggesting that clones active in the early response phases were less likely to be recaptured at later times after treatment. Because we have multiple capture timepoints, we could estimate the lower bound number of clones composing the CAR population by means of mark–recapture statistics, as

previously described[20]. The results suggest that around 34,000 and 55,000 CAR clones might still be in circulation in Pt4 and Pt6, respectively, up to 24/28 months after infusion (Fig. 6b). We then assessed the recapture probability of the expanded T_{SCM} clones observed at early timepoints (Fig. 6c). We found that these clones were different at each follow-up and that some of them were also detected in the early CAR T_{CM}/T_{EM} population, suggesting that this expansion was transient and accompanied by differentiation of the T_{SCM} cells to memory and effector cells. In contrast, these large clones do not seem to have contributed substantially to the pool of long-term-surviving CAR T cells (Fig. 6c).

Importantly, with regard to oncogenic potential of integrated viral vector sequences, we did not observe any major skewing in the distribution of ISs towards gene categories related to T cell growth, activation or survival. In this regard, we identified and tracked 12 clones in our patients bearing an integration in the TET2 gene (Fig. 6d), a locus previously associated with clonal dominance in a single patient with chronic lymphocytic leukemia (CLL) treated with CD19 CAR T cells[17]. Of note, none of these clones showed signs of expansion either in the product or after infusion, contributing to a maximum of 0.044% of sequencing reads out of the total collected in each sample/timepoint (Fig. 6e). Collectively, these data show no evidence of insertional mutagenesis resulting in clonal selection of CAR T cells in these patients, either during the early response phase or in long-term-persisting CAR T cells.

Lastly, we compared these data with results from Pt10 and Pt17. The numbers of unique ISs retrieved in these individuals were broadly similar to those seen in Pt4 and Pt6. In Pt10 and Pt17, we collected 4,633 and 2,823 ISs, respectively, in T_{SCM}, T_{CM} and T_{EM} cells belonging to the cell products, as well as 2,295 and 1,020 ISs, respectively, in T_{SCM} and T_{CM}/T_{EM} cells during the first month of follow-up (Extended Data Fig. 7). We first measured the relative abundance of each IS (Fig. 7a) and analyzed the clonal diversity of the sorted CAR populations from the CAR T cell product and after treatment. As shown in Fig. 7b (top panels), these individuals displayed an overall lower level of clonal diversity in all populations composing the drug product as compared with the patients with long-surviving CAR T cells, and this was particularly evident when analyzing the T_{SCM} compartment. After infusion, we could again observe a clonal burst of CAR T_{SCM} cells during the first month. However, in contrast to the patients with long-term persistence of CAR T cells, the diversity of the T_{CM}/T_{EM} compartments rapidly dropped over the first month in these patients before CAR T cell disappearance (Fig. 7b, bottom panels).

Origin and maintenance of long-term-persisting CAR T cells. Having observed that the long-term-surviving CAR population was composed of a large and stable number of clones of equivalent sizes, we investigated whether we could establish a link between the ISs of the cell product and the ones detected after infusion. Our goal was to understand which of the infused CAR T cell subtypes gave rise to the early expanding and long-term-persisting CAR T cells post-infusion. The depth of our analysis and the number of ISs collected in the product and from the patients allowed us to detect a substantial number of identical ISs in samples collected before and after infusion, for the first time to our knowledge. The sharing of ISs between the CAR T cell product subsets and samples obtained at different timepoints post-infusion is represented in the correlation maps of Fig. 8a. These plots quantify the IS sharing between all samples analyzed, showing in blue dots the paired comparisons where ISs sharing was more substantial (positive correlation). In both patients with long-term persistence, we observed a relatively high frequency of ISs shared among the T subpopulations composing the cell product, suggesting that differentiation has occurred during in vitro expansion at the time of manufacture. Interestingly, we also found a relatively high proportion of ISs shared between the T_{SCM} cells of the product and the T_{SCM} cells isolated at 14 and 30 d after infusion in both patients. This would imply that CAR T_{SCM} cells active during the early CAR T cell response phase are predominantly derived from T_{SCM} cells in the product that have expanded during in vitro manufacture. Notably, T_{SCM} ISs sharing with T_{CM}/T_{EM} cells up to day 30 after treatment ranged between 0.3% and 23%, averaging 8.3%, suggesting active differentiation in the circulation of T_{SCM} cells originally contained in the drug product. In contrast, T_{CM} and T_{EM} cells in the product shared on average a maximum of 2.4% of ISs with the same subtypes up to early timepoints after therapy (range 0.09–7.1), a result in line with the more limited differentiation potential of these memory cell types as compared with T_{SCM} cells.

Despite the detection of identical ISs between the cell product and late timepoints, the IS numbers were not sufficient to reach significance, possibly due to inherent sampling limitations combined with the paucity of CAR T cells still left in circulation in these patients at 6 to 24/28 months after treatment. Nonetheless, the numbers of shared ISs allowed us to investigate the relative contributions of the product subsets to the early and late phases after infusion. As shown in Fig. 8b and Extended Fig. 8, regardless of long-term persistence, in all four patients the majority of the shared integrants at early timepoints were derived from the T_{SCM} CAR T cells in the product, suggesting that this compartment has a key role in early expansion. Similarly, in the patients with long-term persistence, the product subpopulation contributing the most to the clonal pool at late timepoints was the T_{SCM}, from which we collected 46.6% to 60.5% of ISs out of the group of insertions sites detected both in vitro and after infusion. Such a contribution is particularly relevant when one considers the extremely low frequency of T_{SCM} cells observed at the time of infusion (1–2% of total CAR T cells) as compared with T_{CM} or T_{EM} cells.

Discussion

In summary, by combining immunophenotyping and molecular tracking we have gained important insights into the nature and dynamics of both early expanding CAR T cells that mediate initial responses as well as long-term-surviving CAR T cells

Fig. 6 | Tracking of IS in different T cell subtypes over time in Pt4 and Pt6. a, Unsupervised clustering based on IS sharing among subpopulations over time in Pt4 (left panel) and Pt6 (right panel). **b**, Estimation of the number of clones composing the CAR$^+$ cell population in each patient based on the M_{th} Chao lower bound (LB) model applied to IS recapture probability. Shown are individual values and relative standard errors from the abundance model fit estimation (for Pt4, abundance = 34,083 and s.e. = 1,699; for Pt6, abundance = 55,888 and s.e. = 2,795). **c**, Heatmaps showing tracking and relative contribution of T_{SCM} clones (IS, rows) at d14 and d30 recaptured in other T subtypes and timepoints (columns) in Pt4 (top panel) and Pt6 (bottom panel). The intensity of blue is proportional to the relative clone size (IS abundance). **d**, Distribution of IS in proximity to TET2 in both patients combined. The *x* axis displays chromosomal coordinates (base pairs) while the *y* axis displays the IS abundance (log_{10} of percentage) calculated within the population and timepoint where it has been observed. The dark blue bars show IS detected in the patients while red bars show IS detected in the cell product. The transcription start site (TSS), exons (gray boxes) and introns (gray lines) of the TET2 gene are shown on top of the plot in their respective chromosomal locations. **e**, Heatmap showing tracking and relative contribution of the IS shown in panel **d** for each patient in the product (in red) or after infusion (in blue). Relative IS abundance (percentage) calculated within the population and timepoint where it has been observed is reported inside each colored field (white field, not detected).

providing immune surveillance against leukemic relapse in two patients up to 3 yr after infusion. The IS retrieval methodology has been widely used by our group and others as a reliable method for tracking clones, showing added value compared with high-throughput TCR sequencing. This is because (1) it allows a specific tracking of engineered T cell clones even when they are

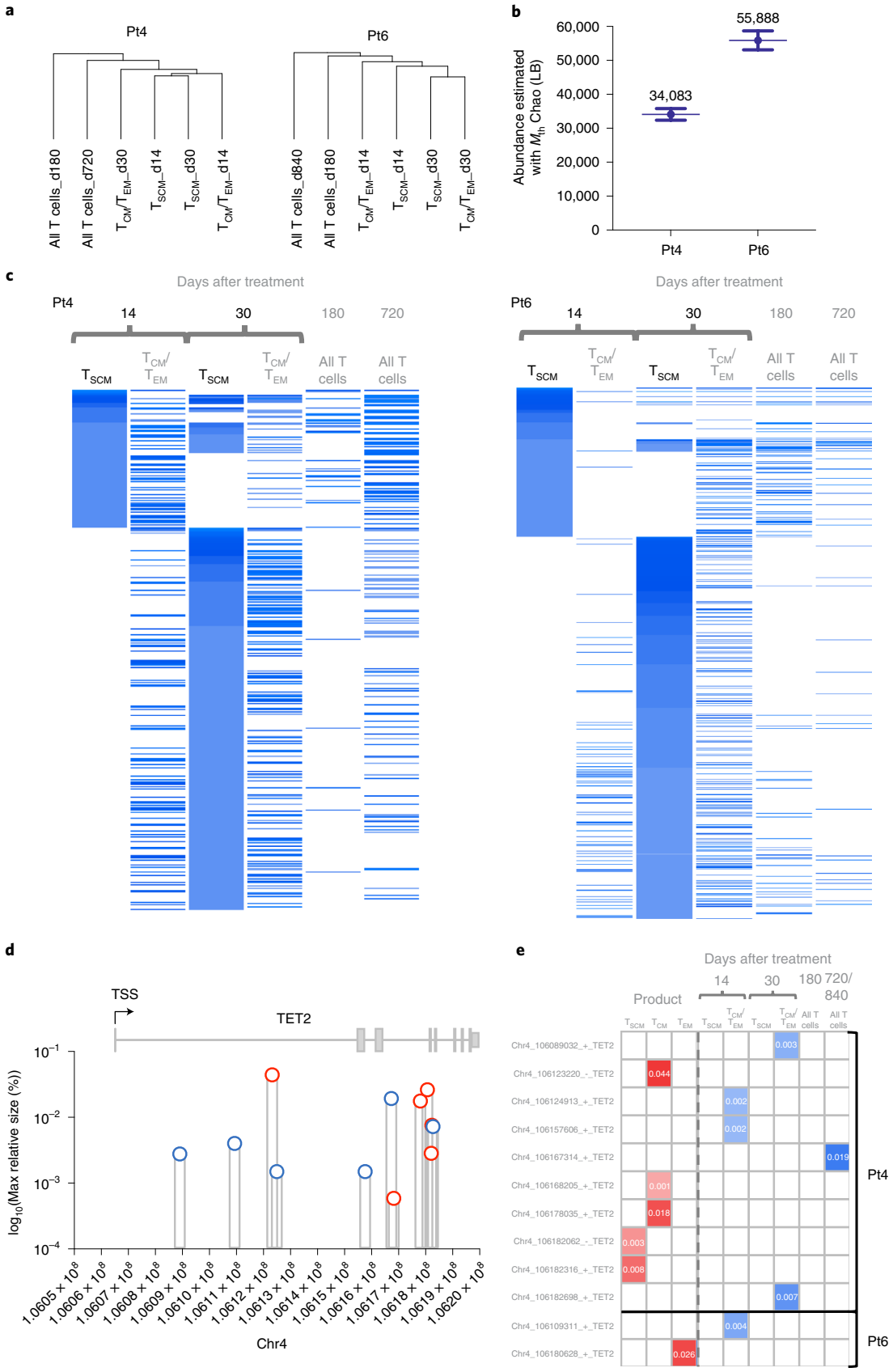

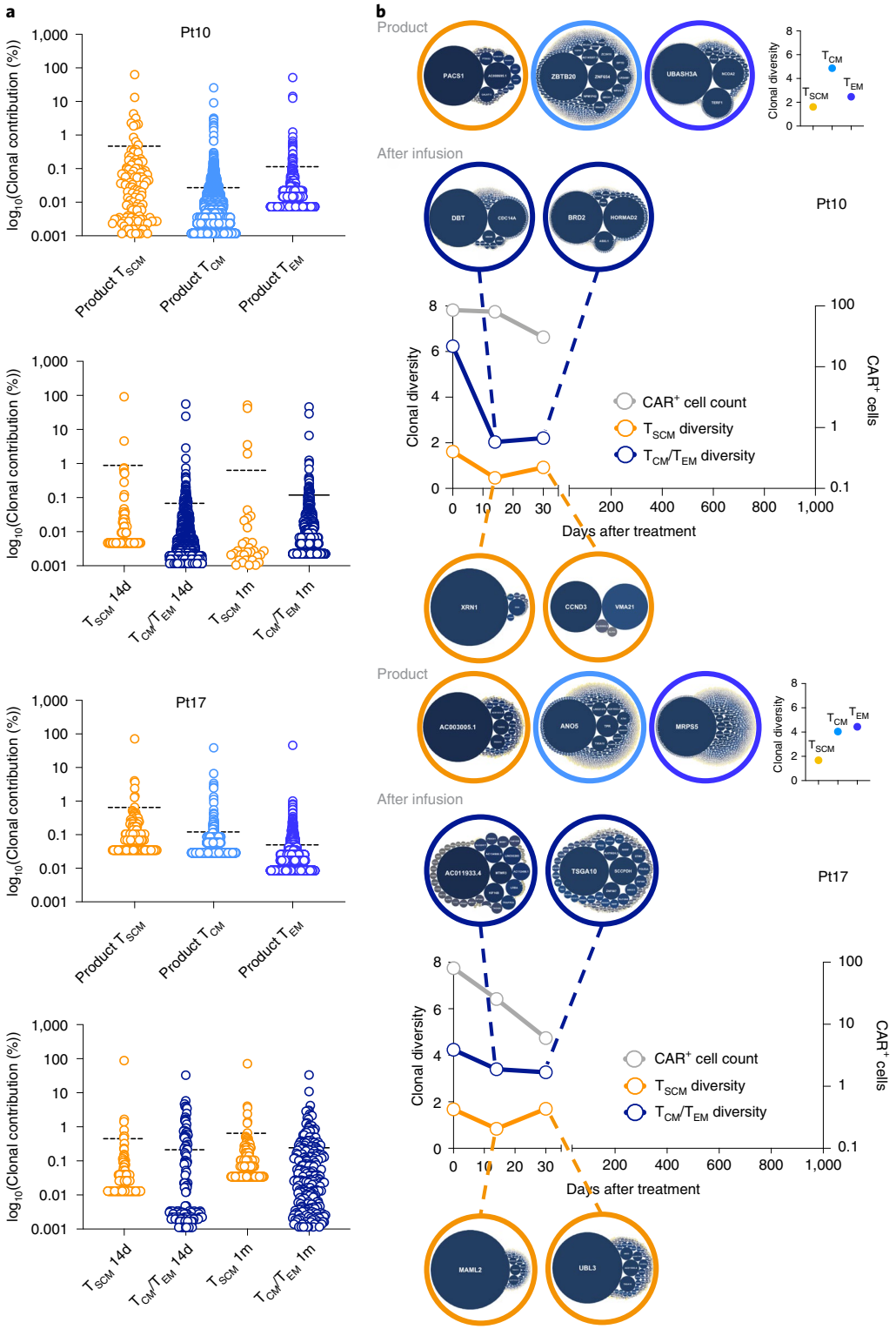

Fig. 7 | Diversity of ISs in different T cell subtypes over time from Pt10 and Pt17. a, Scattered dot plots showing relative abundance of ISs in the product (top section) and at early timepoints (bottom section) after treatment in Pt10 (plots on the top) and Pt17 (plots on the bottom) (d, days after treatment; m, months after treatment). Mean percentage abundance is shown as a dotted line for each sample. Number of events in each dataset is equal to that reported in Extended Data Fig. 7. **b**, Diversity of drug product and CAR cells after infusion in Pt10 (top panels) and Pt17 (bottom panels). Top section, for each product subpopulation analyzed, colored circles (T_{SCM}, orange; T_{CM}, light blue; T_{EM}, blue) contain bubble plots of clones contributing >0.01% to the total population. The dimension of the bubble is proportional to the size of the clone. The name of the gene closest to the relative IS is reported inside the bubble. The plots on the right show Shannon diversity index for each subpopulation. Bottom section, plot showing Shannon diversity index (left *y* axis) of IS over time in T_{SCM} cells (orange lines) and in T_{CM}/T_{EM} cells (dark blue). The gray lines show the percentage of CAR cells over time (right *y* axis). For each timepoint analyzed, colored circles contain bubble plots of clones contributing >0.01% to the total population at each timepoint. The dimension of the bubble is proportional to the size of the clone. The name of the gene closest to the relative IS is reported inside each bubble.

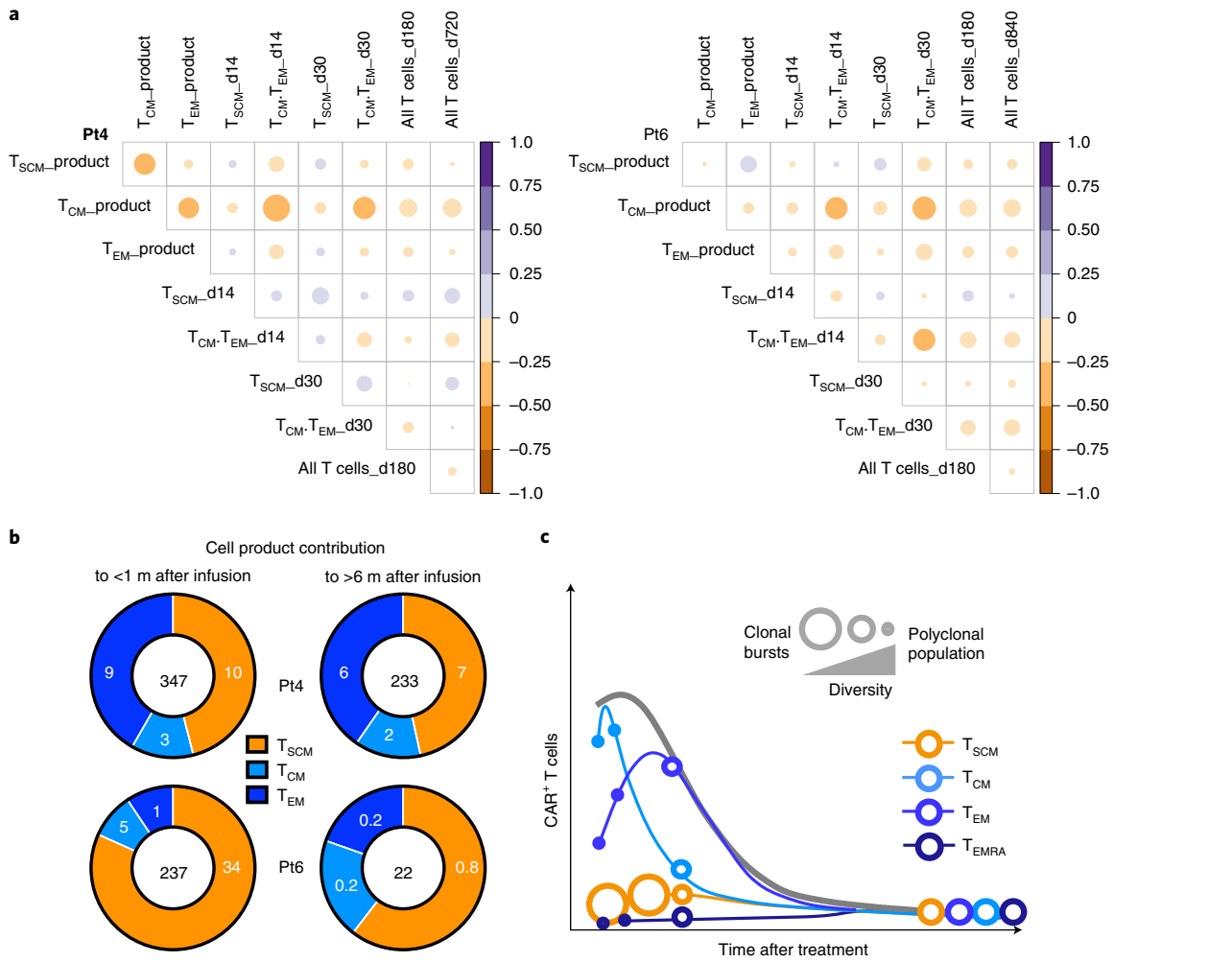

Fig. 8 | Comparison of IS distribution pre- and post-infusion. a, Correlograms showing upper triangle of the correlation matrix among IS datasets from Pt4 (left panel) and Pt6 (right panel). Positive correlations are shown in blue and negative in red. The size of circles is proportional to the correlation value. **b**, Ring plots showing relative contributions from each subtype (colored section of the ring) to the pool of ISs detected in the product and at early (left plots) or late (right plots) timepoints in Pt4 (top panels) and Pt6 (bottom panel). The total numbers of ISs captured both in the product and after infusion are shown inside each plot. The relative percentages of ISs belonging to each T cell subtype of the product that were shared with samples after infusion are shown in white inside each section of each ring plot. **c**, Model summarizing our working hypothesis for CAR T cell dynamics occurring in the patients of this study.

highly diluted in a population of vector-negative cells and therefore in conditions that prevent FACS of CAR cells (such as at late timepoints); and, (2) differently from high-throughput TCR sequencing, it provides a set of stable genomic markers whose relative contribution is independent from the effect of thymic involution, immune tolerance or extrathymic rearrangements. Nonetheless, it should be noted that it is currently impossible to precisely discriminate individual clones based on the assumption 1 IS = 1 clone, since each genetically engineered cell may carry multiple copies of an integrated vector so that interpretation must be based on data trends rather than on the tracking of specific individual ISs or clones.

We show that CAR T cells in the infused product display a polyclonal IS profile and that CAR T cells remain clonally diverse at early and late timepoints post-infusion, with no evidence of clonal dominance. Individual clones showed different patterns of expansion and contraction with time, with different clones responsible for early expansion and long-term persistence. Interestingly, despite having observed several ISs in the TET2 locus, we could not find any sign of clonal expansion of the relevant CAR T cell clones. It should be noted that the TET2 insertional mutagenesis event described by Fraietta et al.[17] was accompanied by a hypomorphic mutation in the second TET2 allele, an extremely rare occurrence which is unlikely to have taken place in the patients analyzed in the present study. It would seem therefore that bi-allelic disruption of the TET2 locus is needed for clonal expansion.

Our results, summarized in the scheme of Fig. 8c, suggest that following infusion, CAR T cells undergo a rapid switch from a predominantly T_{CM} to a T_{EM} phenotype during the early response phases without major clonal imbalance in the memory compartment but with a self-limiting clonal burst phase occurring in the T_{SCM} population. T_{SCM} cells from the infused product can potentially differentiate into other subsets post-infusion. Analysis of shared integrants between the CAR T cell product and after treatment at early (<1 month) timepoints demonstrated that, despite the low frequency of T_{SCM} cells in the products (0.5–2%), a substantial fraction of these clones (10–73%) were responsible for the circulating CAR T cells detected during this early expansion phase in all patients regardless of long-term persistence, implying that differentiation of the oligoclonally expanded T_{SCM} cells into T_{EM} cells may be responsible for much of the early anti-leukemic response. The patients with early loss

of CAR T cells appeared to have a more differentiated phenotype, with a lower proportion of T_{SCM} cells and higher T_{EM} cells as well as reduced clonal diversity in their products. Patients with poor CAR T cell persistence showed markedly reduced clonal diversity in CAR T_{CM} and T_{EM} cells compared with those with long-term persistence. We speculate that when the drug product is more differentiated and less polyclonal, CAR T cells may not be able to preserve a clonal repertoire with enough diversity to avoid exhaustion during the clonal burst associated with the early anti-leukemic response. Further studies in larger patient cohorts are needed, but, if these findings are confirmed, these data have important clinical implications suggesting that assessment of the phenotype and clonal diversity of the product and at early timepoints may identify patients at high risk of early CAR T cell loss who may benefit from consolidative transplant.

In the patients with long-term CAR T cell persistence, CAR T cells did not terminally differentiate into T_{EMRA} cells upon exposure to CD19 antigen, but instead the T_{SCM} phenotype became more prevalent over time concomitantly with long-term maintenance of clonal diversity. We can therefore speculate that long-term maintenance of CAR T cells is supported by self-renewing cells endowed with homeostatic proliferative capacity such as T_{SCM} cells. Critically, we could estimate that clones belonging to the small fraction of T_{SCM} cells present in the cell product at the time of infusion had the highest recapture probability within the pool of long-lived CAR^+ T cells in circulation, proving for the first time, to our knowledge, the crucial role of T_{SCM} cells in long-term anti-leukemic surveillance by CAR T cells.

Our working hypothesis is that the remarkable early expansion and persistence of our CAR T cell product achieved in Pt4 and Pt6 reflects a combination of two key factors. Firstly, our previous preclinical data[16] both in vitro and in a xenogeneic mouse model suggested that signaling through our low-affinity CAR molecule CAT-19 (CAT) CAR results in enhanced CAR T cell expansion which may in part be mediated through higher expression of IL-7R and Bcl-2, promoting homeostatic proliferation and preventing apoptosis. Moreover, the faster off rate with this CAR could potentially have reduced differentiation of CAR T cells during the early anti-leukemic response, preventing terminal differentiation and allowing self-renewal of CAR T_{SCM} cells capable of long-term survival. Our CAR construct incorporated a 4–1BB costimulatory domain, which may confer prolonged persistence compared with CD28 by preventing exhaustion through tonic signaling[21,22]. Secondly, our manufacturing protocol was relatively short (7–8 d) and did not utilize exogenous cytokines in the medium, which may favor less in vitro differentiation and preservation of high levels of T_{CM} cells whose expansion potential could have contributed to an enhanced early response. These culture conditions allowed a small fraction of T_{SCM} cells to be infused in those patients in large enough doses to survive the initial clonal burst phases and to maintain a pool of CAR^+ cells long term.

There are clearly some unavoidable technical constraints to the data reported in this study, including the limited number of patients in whom material was available, the stability of the CD62L marker upon cell culture which could introduce a bias in the estimation of T_{SCM}/T_{CM} cells in the drug product, the low frequency of circulating CAR T cells at late timepoints, the potential sampling biases and the surrogate nature of clonal size quantification based on sequencing abundance of each IS, as a consequence of uneven amplifications of vector–genome junctions[23].

Despite these limitations, our data provide evidence for the first time, to our knowledge, of the critical role of T_{SCM} cells in mediating both early anti-leukemic responses and long-term persistence of CAR T cells after infusion. Future efforts will focus on validating these findings in larger patient cohorts and improvement of CAR design and manufacturing methodology to preserve T_{SCM} and T_{CM} cells in the infused cell product.

Methods

Patients. The CARPALL study (NCT02443831) was approved by the UK Medicines and Healthcare Products Regulatory Agency (clinical trial authorization no. 20363/0361/001) and ethical approval (including the research in this manuscript) was obtained from the London West London & Gene Therapy Advisory Committee (GTAC) Research Ethics Committee (REC ref. no. 16/LO/0283). Written, informed consent was obtained from patients or their parents/guardians before study entry. All patients had relapsed $CD19^+$ ALL and three had relapsed post-bone marrow transplant (BMT). Pt4 and Pt6 had long-term persistence of CAR T cells associated with ongoing durable complete remissions, whereas Pt10 and Pt17 had early loss of CAR T cells. Pt4 is a 21-yr-old man who had a combined bone marrow and central nervous system (CNS) relapse 1 yr post-transplant of matched unrelated donor peripheral blood stem cells and was treated with 10^6 CAR T cells per kg in the third complete remission (CR) (molecular minimal residual disease (MRD) 2.6×10^{-5}) on 23 November 2016. He is currently well and in molecular CR with detectable circulating CAR T cells 3.5 yr post-infusion. Pt6 is an 11-yr-old boy who had a combined bone marrow and CNS relapse 14 months after a matched unrelated donor BMT for ALL and relapsed again in the cerebrospinal fluid (CSF) with molecular disease in the bone marrow 7 months after the second BMT. He was treated with 10^6 CAR T cells per kg (molecular MRD 5×10^{-4}) on 5 October 2016 and remains well and in molecular CR with detectable circulating CAR T cells 3.5 yr post-infusion. Pt10 was a 10-yr-old boy with an isolated bone marrow relapse 17 months after matched family donor BMT who was treated with 10^6 CAR T cells per kg in the third CR (molecular MRD 3×10^{-5}) on 30 August 2017 and had molecular CR and excellent initial CAR T cell expansion at 1 month, but CAR T cells were undetectable by flow and quantitative PCR from 2 months post-infusion. He relapsed with CD19 disease 7 months post CAR T cell therapy and subsequently died of a fungal infection. Pt17 is a 15-yr-old boy with late isolated CNS relapse who relapsed again in the CNS despite cranial irradiation and was treated with 10^6 CAR T cells per kg in the third CR (molecular MRD 5×10^{-5} negative) on 25 July 2018 and had continuing molecular CR and excellent initial CAR T cell expansion at 1 month, but CAR T cells were undetectable by flow and quantitative PCR from 4 months. He was consolidated with a mismatched unrelated donor BMT and remains in CR at 2 yr post-transplant. The average viral copy number per cell for the infused CAR T cell product for Pt4, Pt6, Pt10 and Pt17 was 8, 3.8, 4.9 and 5.6, respectively.

Characterization and isolation of lymphoid and myeloid cells. We performed immunophenotyping on whole-blood EDTA samples while cell sorting was performed on peripheral blood mononuclear cells (PBMCs) isolated from the whole blood by density gradient centrifugation using LymphoPrep (Sigma) after dextran sedimentation. For sorting, PBMCs were thawed in RPMI (10% FCS) pre-warmed with DNase 200 µl ml^{-1} (also used TexMACS 5% human AB serum). Cells were then washed, counted and stained on ice in 100 µl of PBS for every 5×10^6 cells. First, Fc block (BD 564220, 5 µl) was applied for 10 min and, without washing, an anti-idiotype CD19 CAT19 B12RIgG2a (Evitria) (2.5 µl or 3.5 µg) was added for 20 min. Then cells were washed and stained for 30 min with secondary antibody mix containing anti-rat IgG PE for CAR detection (Biolegend 405406, 0.5 µl), CD3 APC-Cy7 (Biolegend 300426, 5 µl), 7-AAD (BD 555816, 5 µl), CD95 BV711 (BD 563132, 5 µl), CD45RA v450 (BD 8053598, 2 µl) and CD62L APC (Biolegend 304810, 3 µl). Cells were washed, resuspended in sorting buffer (PBS (1% FBS) + 1 mM EDTA), passed through a cell strainer (30–40 µM) and then sorted using a FASCAriaIII cell sorter. Raw FACS data were collected using DIVA software (BD Biosciences) and analyzed with FlowJo (TreeStar). When feasible, an aliquot of the sorted cells was re-run through the cell sorter to check fraction purity.

DNA extraction and genome amplification. We performed DNA extraction using QIAamp DNA Blood Mini Kit (Qiagen) for samples of 10,000 to 5×10^6 cells and MN NucleoSpin Tissue XS Kit (MN) for up to 10,000 cells, according to the manufacturers' instructions. Genomic DNA was quantified using a Nanodrop One Spectrophotometer (ThermoFisher). For IS analysis, a whole-genome amplification was performed if the DNA yield after extraction was lower than 300 ng using the Qiagen Repli-G Mini Kit (Manufacturer), according to the manufacturer's instructions.

IS collection and library preparation. For vector IS analysis, we used linear amplification-mediated PCR combined with high-throughput sequencing as previously described[5,20]. Briefly, two rounds of linear PCR were performed (50 cycles each) to enrich for vector–genome junctions using biotinylated primers specific for vector long terminal repeats (LTRs). Streptavidin-coupled magnetic beads (Invitrogen Dynabeads Kilobase Binder Kit) were added to each sample, to capture linearly amplified fragments, followed by complementary strand synthesis. Samples then underwent restriction enzyme digestion using three different enzymes, MluCI, AciI or HpyCH4IV, to minimize bias and improve genome coverage. Linker cassettes were ligated to these fragments, then samples underwent two rounds of exponential amplification PCR to amplify fragments containing vector LTR and linker cassette sequences. PCR fragment size depends on the distance between the known vector sequence and the closest enzyme

recognition site. To visualize amplified fragments, we used high-resolution gel electrophoresis (ElchromScientific). Final PCR products were purified with QIAQUICK PCR Purification Kit (QIAGEN). Fusion PCR was used to add customized sequence-specific Illumina adaptors to the final PCR products. Different combinations of sample barcodes included in both LTR adaptors and linker cassette (LC) adaptors were used to differentiate between different samples.

Computational analyses of IS data. IS identification and analysis were performed through a custom analytical pipeline extensively described in previous publications[5,18–20]. Briefly, raw IS datasets underwent a series of different bioinformatics filtering procedures according to the type of analysis to be performed. All datasets were processed with a 'collision detection filter' to univocally assign each IS to a patient and to one or more T cell subpopulations by applying a tenfold rule for contamination identification as previously reported[5]. A final matrix M was generated where each row r represented an individual IS while each column c represented an individual cell type/sample and timepoint. Each entry of M contained the abundance of each r for each c in terms of sequencing reads. The data shown in Figs. 3–7 and Extended Data Figs. 2–8 were generated on the basis of the IS databases attached as Source data. Graphical representations of IS analyses were generated with Prism8 (GraphPad Software) unless otherwise specified below. Panels in Fig. 3 were generated using the Circos software (http://circos.ca). Word clouds in Fig. 3 and Extended Data Fig. 4 were generated on the basis of the relative incidence of the single closest gene to each IS and plotted using the online suite WordClouds (https://www.wordclouds.com). Panels with lines in Figs. 4, 5 and 7b and Extended Data Fig. 1 were created by plotting IS diversity over time calculated as Shannon diversity or Gini–Simpson index through the R package BiodiversityR (https://cran.r-project.org/web/packages/BiodiversityR/index.html). The 'bubble' plots in Figs. 4, 5 and 7b were created on the basis of the IS with abundance >0.01% relative to each subpopulation and timepoint using the R package packcircles (https://cran.r-project.org/web/packages/packcircles/index.html). The dendrograms in Fig. 6a were generated based on the similarity among IS datasets through the hclust function (https://www.rdocumentation.org/packages/fastcluster/versions/1.1.25/topics/hclust). Estimations of clonal abundance and standard errors shown in Fig. 6b were calculated by the conversion of M to an $M(0,1)$ matrix of incidence and by the application to $M(0,1)$ of log-linear models for closed populations through the R package Rcapture (https://cran.r-project.org/web/packages/Rcapture/index.html, function = closedp.t). The M_{th} (model for abundance estimate with time and heterogeneity effects) Chao LB method was selected for visualization in Fig. 6b, being the most conservative estimation among the ones with the lowest Bayesian information content. The heatmaps in Fig. 6c,e were generated through the use of the R package gplots (https://cran.r-project.org/web/packages/gplots/index.html). The correlograms in Fig. 8a were generated using the R package corrplot (https://cran.r-project.org/web/packages/corrplot/corrplot.pdf). Correlation values for both plots were generated through the function Mcorr. The IS distribution around transcription start sites, the gene content of IS loci shown in Extended Data Fig. 3 and the Gene Ontology analysis of hit genes shown in Extended Data Fig. 3 (right panels) were generated through the online suite GREAT (Genomic Regions Enrichment of Annotations Tool) (http://great.stanford.edu/public/html/) using BED data from IS coordinates, associating genomic regions with the rule of single nearest gene within 1,000 kilobases to each IS and applying the gene annotations to these regions.

Statistics and reproducibility. No statistical method was used to predetermine sample size. The experiments were not randomized, and no data were excluded from the analyses.

Reporting Summary. Further information on research design is available in the Nature Research Reporting Summary linked to this article.

Data availability

The fastq files relative to sequencing of IS amplicons generated for this study are available through the NCBI repository (https://submit.ncbi.nlm.nih.gov/), BioProject accession number PRJNA718947. Source data are provided with this paper. All other data supporting the findings of this study are available from the corresponding author on reasonable request.

Code availability

No new code was generated or used in this manuscript.

Received: 7 July 2020; Accepted: 7 April 2021;
Published online: 24 May 2021

References

1. Sallusto, F., Lenig, D., Förster, R., Lipp, M. & Lanzavecchia, A. Two subsets of memory T lymphocytes with distinct homing potentials and effector functions. *Nature* https://doi.org/10.1038/35005534 (1999).
2. Gattinoni, L. et al. A human memory T cell subset with stem cell-like properties. *Nat. Med.* **17**, 1290–1297 (2011).
3. Heslop, H. E. et al. Long-term outcome of EBV-specific T-cell infusions to prevent or treat EBV-related lymphoproliferative disease in transplant recipients. *Blood* https://doi.org/10.1182/blood-2009-08-239186 (2010).
4. Berger, C. et al. Adoptive transfer of effector CD8$^+$ T cells derived from central memory cells establishes persistent T cell memory in primates. *J. Clin. Invest*. https://doi.org/10.1172/JCI32103 (2008).
5. Biasco, L. et al. In vivo tracking of T cells in humans unveils decade-long survival and activity of genetically modified T memory stem cells. *Sci. Transl. Med.* **7**, 273ra13 (2015).
6. Oliveira, G. et al. Tracking genetically engineered lymphocytes long-term reveals the dynamics of T cell immunological memory. *Sci. Transl. Med.* **7**, 317ra198 (2015).
7. Maude, S. L. et al. Chimeric antigen receptor T cells for sustained remissions in leukemia. *N. Engl. J. Med*. https://doi.org/10.1056/NEJMoa1407222 (2014).
8. Lee, D. W. et al. T cells expressing CD19 chimeric antigen receptors for acute lymphoblastic leukaemia in children and young adults: a phase 1 dose-escalation trial. *Lancet* https://doi.org/10.1016/S0140-6736(14)61403-3 (2015).
9. Gardner, R. A. et al. Intent-to-treat leukemia remission by CD19 CAR T cells of defined formulation and dose in children and young adults. *Blood* https://doi.org/10.1182/blood-2017-02-769208 (2017).
10. Maude, S. L. et al. Tisagenlecleucel in children and young adults with B-cell lymphoblastic leukemia. *N. Engl. J. Med*. https://doi.org/10.1056/NEJMoa1709866 (2018).
11. Mueller, K. T. et al. Cellular kinetics of CTL019 in relapsed/refractory B-cell acute lymphoblastic leukemia and chronic lymphocytic leukemia. *Blood* https://doi.org/10.1182/blood-2017-06-786129 (2017).
12. Sommermeyer, D. et al. Chimeric antigen receptor-modified T cells derived from defined CD8$^+$ and CD4$^+$ subsets confer superior antitumor reactivity in vivo. *Leukemia* https://doi.org/10.1038/leu.2015.247 (2016).
13. Turtle, C. J. et al. CD19 CAR-T cells of defined CD4$^+$:CD8$^+$ composition in adult B cell ALL patients. *J. Clin. Invest*. https://doi.org/10.1172/JCI85309 (2016).
14. Xu, Y. et al. Closely related T-memory stem cells correlate with in vivo expansion of CAR.CD19-T cells and are preserved by IL-7 and IL-15. *Blood* https://doi.org/10.1182/blood-2014-01-552174 (2014).
15. Sheih, A. et al. Clonal kinetics and single-cell transcriptional profiling of CAR-T cells in patients undergoing CD19 CAR-T immunotherapy. *Nat. Commun.* **11**, 219 (2020).
16. Ghorashian, S. et al. Enhanced CAR T cell expansion and prolonged persistence in pediatric patients with ALL treated with a low-affinity CD19 CAR. *Nat. Med*. https://doi.org/10.1038/s41591-019-0549-5 (2019).
17. Fraietta, J. A. et al. Disruption of TET2 promotes the therapeutic efficacy of CD19-targeted T cells. *Nature* https://doi.org/10.1038/s41586-018-0178-z (2018).
18. Aiuti, A. et al. Lentiviral hematopoietic stem cell gene therapy in patients with Wiskott-Aldrich syndrome. *Science* **341**, 6148 (2013).
19. Scala, S. et al. Dynamics of genetically engineered hematopoietic stem and progenitor cells after autologous transplantation in humans. *Nat. Med.* **24**, 1683–1690 (2018).
20. Biasco, L. et al. In vivo tracking of human hematopoiesis reveals patterns of clonal dynamics during early and steady-state reconstitution phases. *Cell Stem Cell* **19**, 107–119 (2016).
21. Milone, M. C. et al. Chimeric receptors containing CD137 signal transduction domains mediate enhanced survival of T cells and increased antileukemic efficacy in vivo. *Mol. Ther*. https://doi.org/10.1038/mt.2009.83 (2009).
22. Long, A. H. et al. 4-1BB costimulation ameliorates T cell exhaustion induced by tonic signaling of chimeric antigen receptors. *Nat. Med*. https://doi.org/10.1038/nm.3838 (2015).
23. Biasco, L. Integration site analysis in gene therapy patients: expectations and reality. *Hum. Gene Ther.* **28**, 1122–1129 (2017).

Acknowledgements

This work was funded the JP Moulton Foundation and supported by the National Institute for Health Research Biomedical Research Centre at Great Ormond Street Hospital for Children NHS Foundation Trust and University College London. P.J.A. is a recipient of an NIHR Research Professorship which also supported S.G. M.P. is supported by the National Institute of Health Research University College London Hospital Biomedical Research Centre. A.J.T. is a recipient of a Wellcome Trust Senior Fellowship. The work of L.B. was supported by the Wellcome Trust (grant no. 104807/Z/14/Z, Principal Research Fellowship awarded to A.J.T.) and the National Institute for Health Research Biomedical Research Centre at Great Ormond Street Hospital for Children NHS Foundation Trust, London, UK. L.B. is also currently Director of R&D for the gene therapy company AVROBIO located in Cambridge, MA, USA (none of what is presented in this work is supported by or relates to AVROBIO). The work of L.B. was also in part performed using the resources of the Gene Therapy Program of the Dana Farber/Boston Children's Cancer and Blood Disorders Center.

Author contributions

L.B. designed and co-supervised the study, performed computational analyses and wrote the manuscript. N.I. and C.R. performed cell isolation and molecular insertion sites retrieval. S.G. and R.R. collected and provided clinical sample material for analysis. A.G. cryopreserved study samples and performed flow cytometric staining. R.H. and R.W. were Principal Investigators for the clinical study. B.P. wrote study documentation and provided trial management. A.L. provided statistical analysis for the study. M.P. generated the CAR construct and participated in its preclinical characterization. A.J.T. conceived the idea and participated in the experimental design and data analysis. P.J.A. supervised the study as PI and wrote the manuscript.

Competing interests

The authors declare no competing interests.

Additional information

Extended data is available for this paper at https://doi.org/10.1038/s43018-021-00207-7.

Supplementary information The online version contains supplementary material available at https://doi.org/10.1038/s43018-021-00207-7.

Correspondence and requests for materials should be addressed to P.J.A.

Peer review information *Nature Cancer* thanks Justin Eyquem, Alena Gros and the other, anonymous, reviewer(s) for their contribution to the peer review of this work.' after the Supplementary information section.

Reprints and permissions information is available at www.nature.com/reprints.

Publisher's note Springer Nature remains neutral with regard to jurisdictional claims in published maps and institutional affiliations.

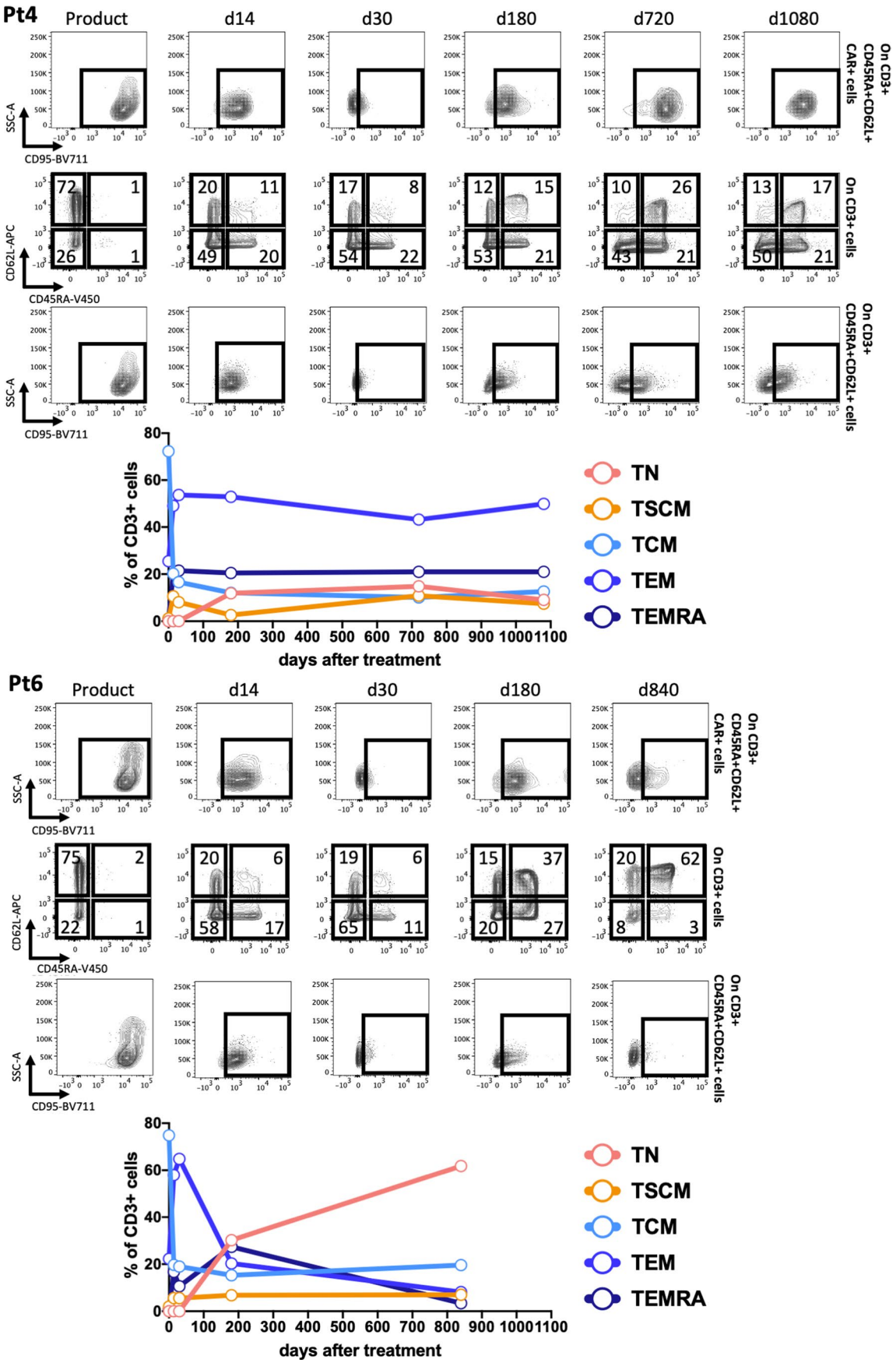

Extended Data Fig. 1 | See next page for caption.

Extended Data Fig. 1 | Immunophenotyping of CD3+ cells in Pt4 and Pt6. Additional FACS plot on CD62L+CD45RA+CD95 expression in CAR$^+$ T cells, subtype frequencies within total CD3$^+$ cells and relative summary of data on the CD3$^+$ T cell composition overtime for Pt4 (top panels) and Pt6 (bottom panels). Percentages of CD62L/CD45RA compartments are showed inside each gate. Longitudinal contribution of each subpopulations to the CD3$^+$ cell compartment is shown below for each patient according to the color code legend on the right.

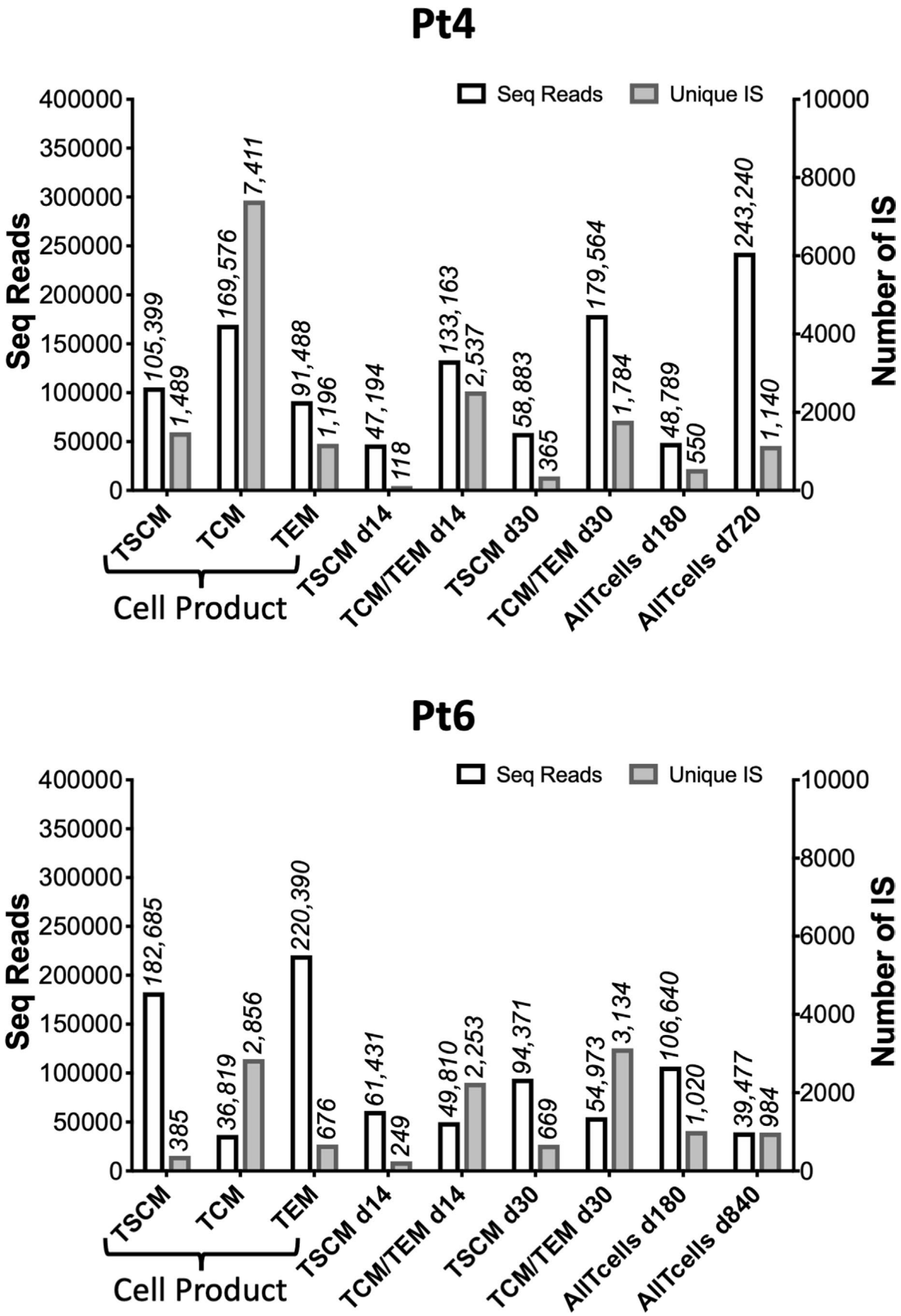

Extended Data Fig. 2 | Integration sites collected from Pt4 and Pt6. Summary of number of IS (grey bars) and relative sequencing reads (white bars) in Pt4 (top panel) and Pt6 (bottom panel) (d = days after treatment).

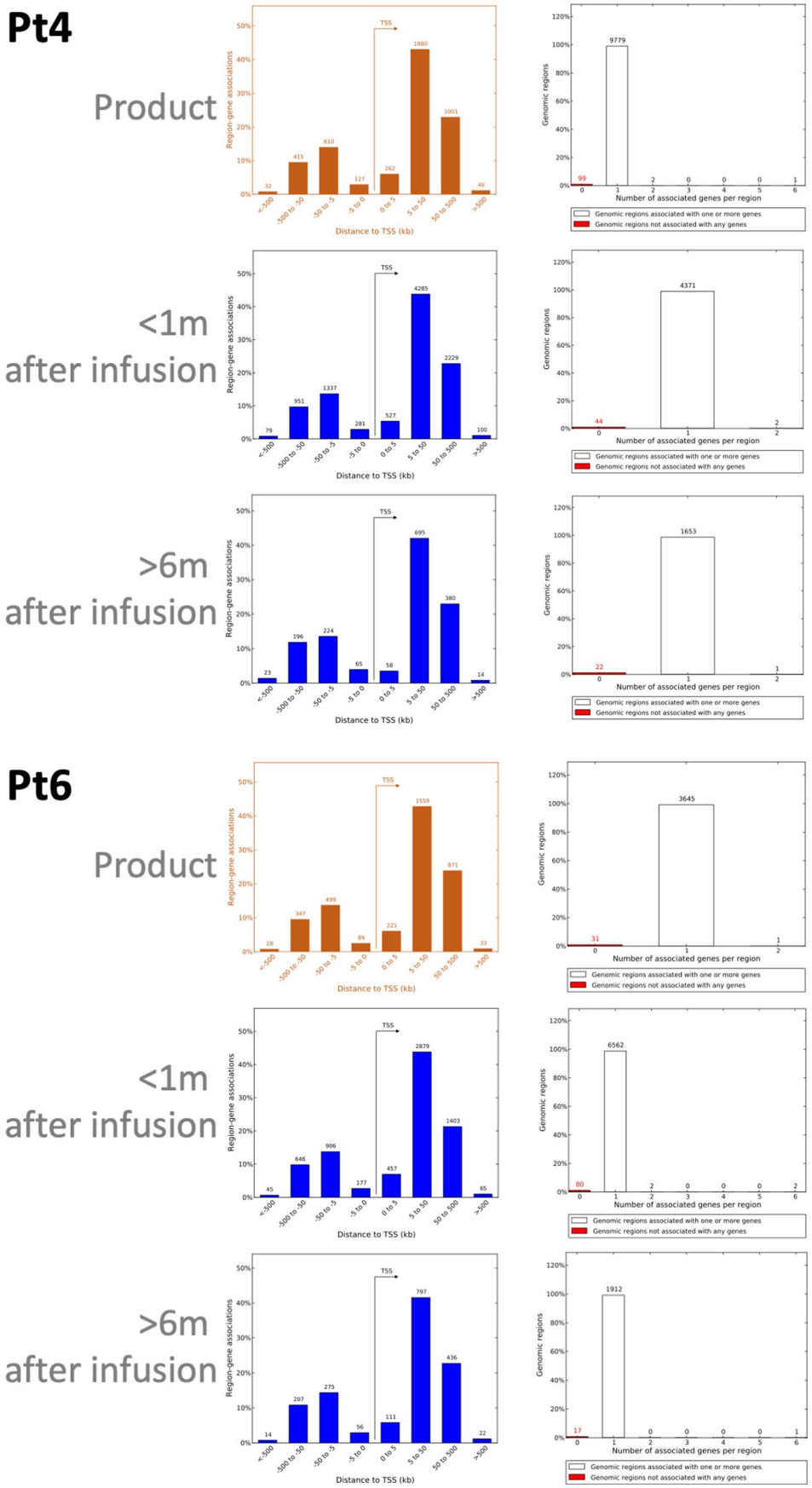

Extended Data Fig. 3 | Distribution of integration sites collected from Pt4 and Pt6. Distribution of IS with respect to TSS (left plots) or gene content of the loci (right plots) in the cell product (red) or after infusion at early or late timepoints after treatment (blue) for Pt4 (top panels) and Pt6 (bottom panels).

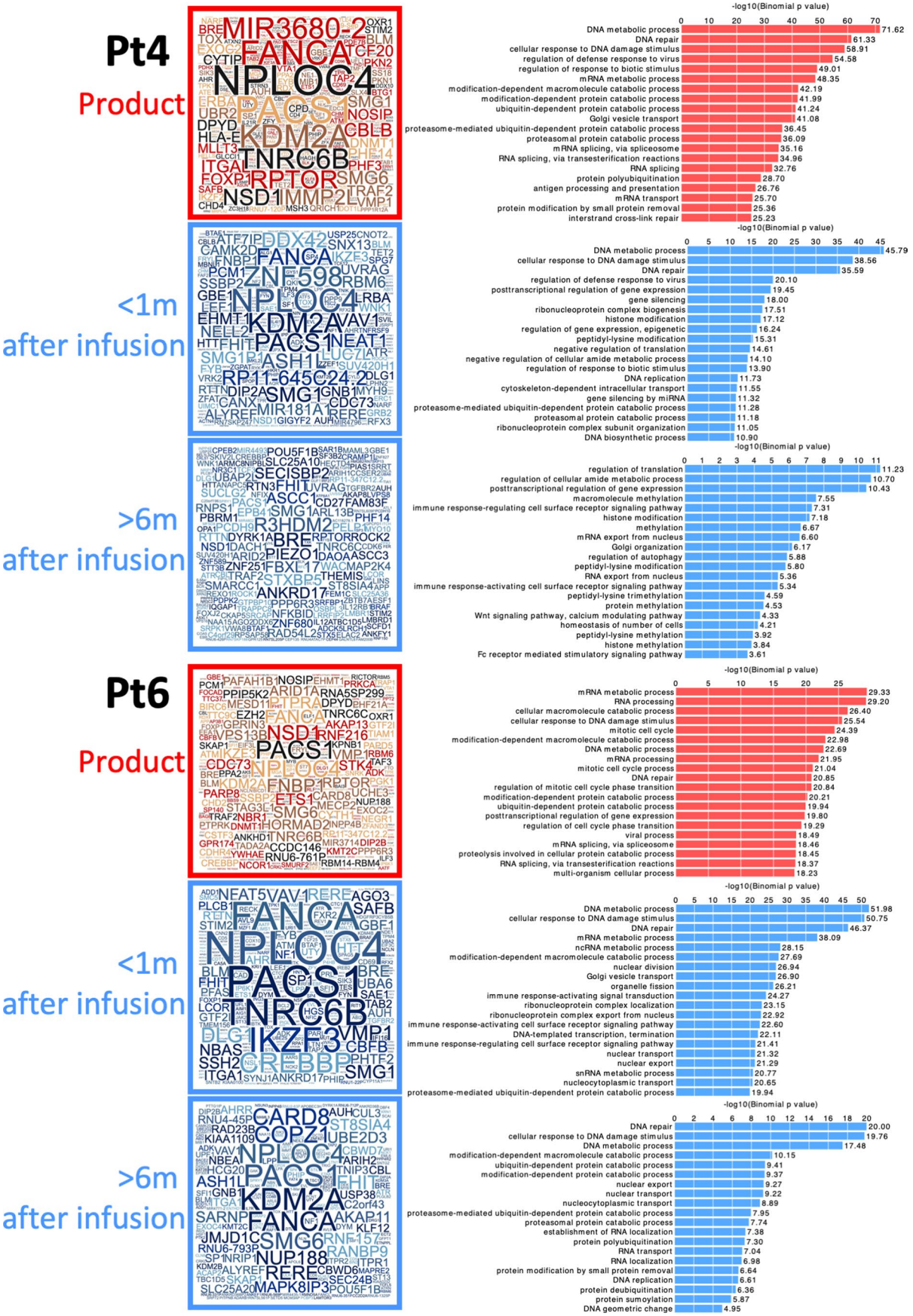

Extended Data Fig. 4 | See next page for caption.

Extended Data Fig. 4 | Gene categories relative to integration sites collected from Pt4 and Pt6. Plots on the left show word clouds of hit genes in the cell product (in red) and after infusion at early or late timepoints after treatment (in blue) for Pt4 (top panels) and Pt6 (bottom panels). Relative gene enrichment analysis for top biological processes of hit genes relative to each word cloud in the product (red bars) or after infusion (blue bars) is shown on the right plots (significance reported as -log10 binomial p-value from one-tailed tests decreasing from top to bottom).

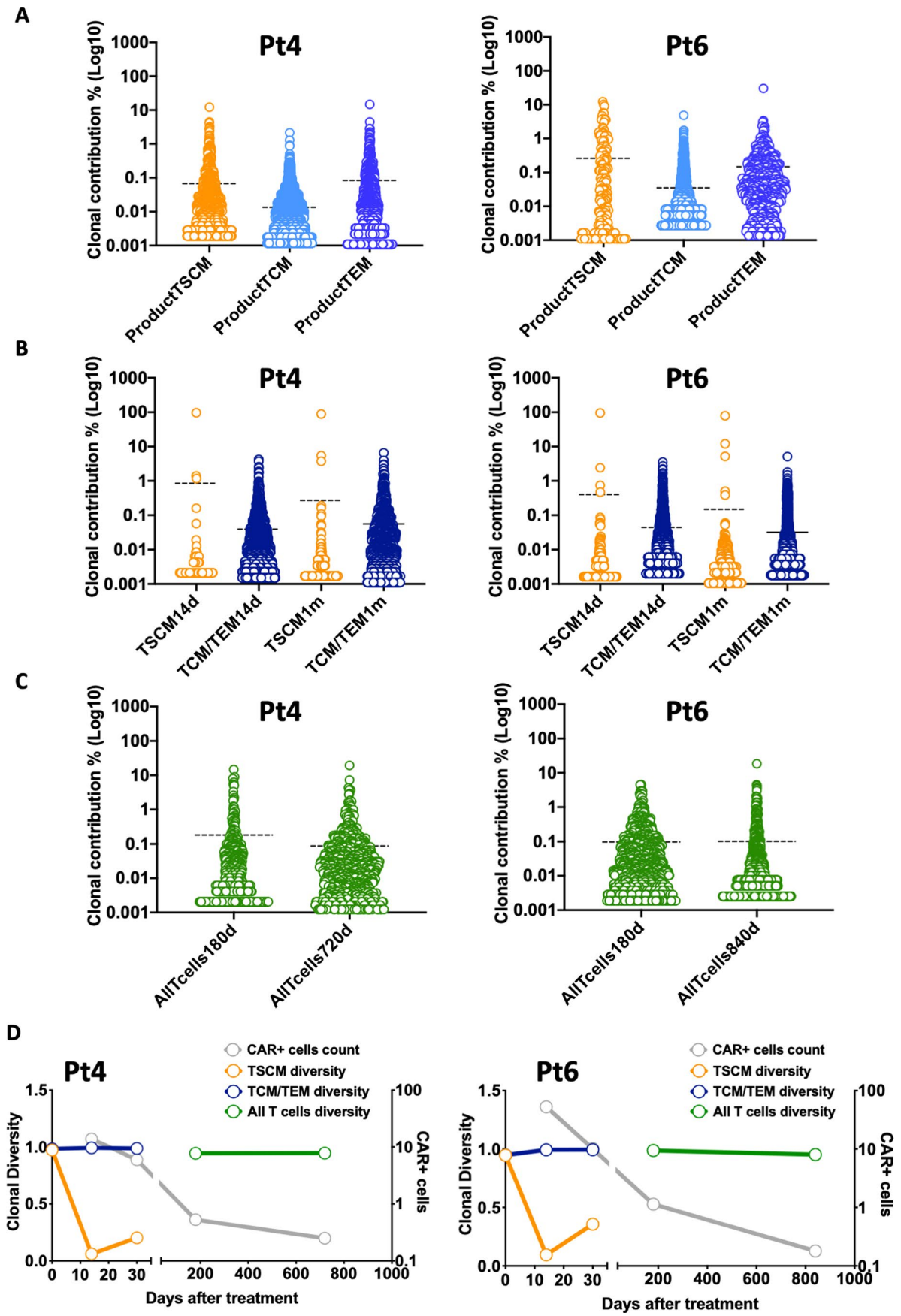

Extended Data Fig. 5 | See next page for caption.

Extended Data Fig. 5 | Relative abundance and diversity of integration sites collected from Pt4 and Pt6. Scattered dot plots showing relative abundance of IS in the product (**a**) and at early (**b**) or late (**c**) timepoints after treatment in Pt4 (plots on the left) and Pt6 (plots on the right) (d = days after treatment, m = months after treatment). Mean percent abundance is shown as a dotted line for each sample. Number of events in each dataset is equal to what reported in Extended Data Fig. 2. **d**) Longitudinal plots showing Gini/Simpson Diversity Index (left y-axis) of IS overtime in T_{SCM} (orange lines) and in T_{CM}/T_{EM} (dark blue) and in all T cells (green lines). The grey lines show the percentage of CAR cells overtime (right y-axis).

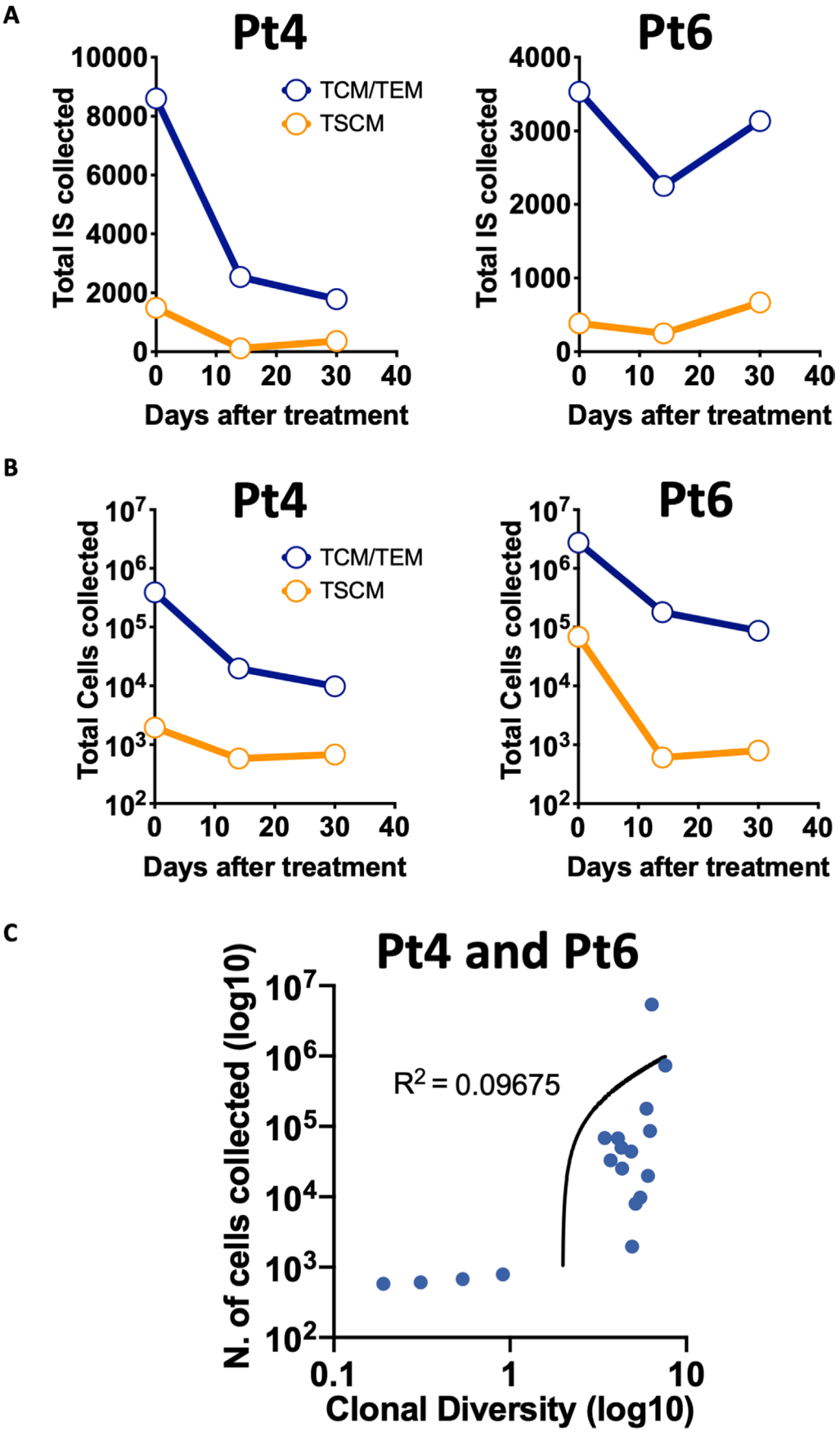

Extended Data Fig. 6 | See next page for caption.

Extended Data Fig. 6 | Correlation of integration sites and number of cells collected from Pt4 and Pt6. Longitudinal plots showing number of IS collected (**a**) and number of cells collected (**b**) in T_{SCM} (orange lines) and in T_{CM}/T_{EM} (dark blue) at early timepoints for Pt4 (left panels) and Pt6 (right panels). The plot in (**c**) shows the correlation observed between number of cells collected (y-axis) and clonal diversity for all samples and both patients (x-axis, Shannon Diversity Index) shown as blue dots. Interpolation with best fit curve and R squared value are shown in black.

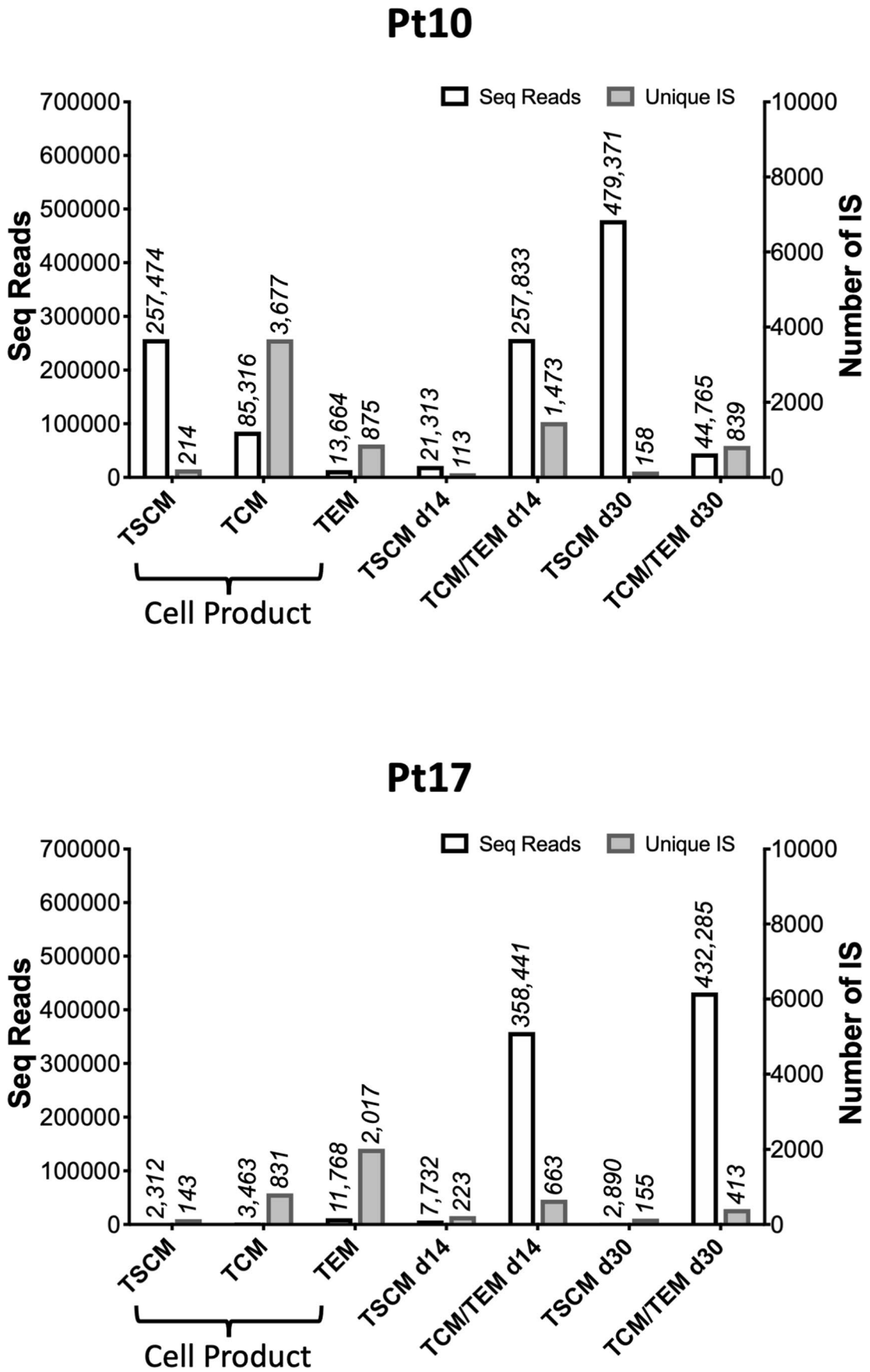

Extended Data Fig. 7 | Integration sites collected from Pt10 and Pt17. Summary of number of IS (grey bars) and relative sequencing reads (white bars) in Pt10 (top panel) and Pt17 (bottom panel) (d = days after treatment).

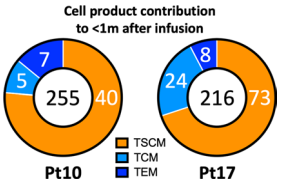

Extended Data Fig. 8 | Sharing of integration sites in the product with the CAR T populations in Pt10 and Pt17 after infusion. Ring plots showing relative contribution from each subtype (coloured section of the ring) to the pool of IS detected in the product and at early timepoints in Pt10 (left) and Pt6 (right). The total number of IS captured both in the product and after infusion is shown inside each plot. The relative percentage of IS belonging to each T cell subtype of the product that were shared with samples after infusion is shown in white inside each section of each ring plot.

nature research

Corresponding author(s): Persis Amrolia

Last updated by author(s): Jul 14, 2020

Reporting Summary

Nature Research wishes to improve the reproducibility of the work that we publish. This form provides structure for consistency and transparency in reporting. For further information on Nature Research policies, see our Editorial Policies and the Editorial Policy Checklist.

Statistics

For all statistical analyses, confirm that the following items are present in the figure legend, table legend, main text, or Methods section.

n/a	Confirmed	
☐	☒	The exact sample size (*n*) for each experimental group/condition, given as a discrete number and unit of measurement
☐	☒	A statement on whether measurements were taken from distinct samples or whether the same sample was measured repeatedly
☐	☒	The statistical test(s) used AND whether they are one- or two-sided *Only common tests should be described solely by name; describe more complex techniques in the Methods section.*
☒	☐	A description of all covariates tested
☒	☐	A description of any assumptions or corrections, such as tests of normality and adjustment for multiple comparisons
☐	☒	A full description of the statistical parameters including central tendency (e.g. means) or other basic estimates (e.g. regression coefficient) AND variation (e.g. standard deviation) or associated estimates of uncertainty (e.g. confidence intervals)
☐	☒	For null hypothesis testing, the test statistic (e.g. *F*, *t*, *r*) with confidence intervals, effect sizes, degrees of freedom and *P* value noted *Give P values as exact values whenever suitable.*
☒	☐	For Bayesian analysis, information on the choice of priors and Markov chain Monte Carlo settings
☒	☐	For hierarchical and complex designs, identification of the appropriate level for tests and full reporting of outcomes
☒	☐	Estimates of effect sizes (e.g. Cohen's *d*, Pearson's *r*), indicating how they were calculated

Our web collection on statistics for biologists contains articles on many of the points above.

Software and code

Policy information about availability of computer code

Data collection	Immunophenotyping: FACS raw data were collected through DIVA software (BD Bioscience). IS analysis: Custom code required for IS mapping was already described in Biasco et al. Cell Stem Cell 2016. Raw integration sites data sets underwent series of different bioinformatical filtering procedures according to the type of analysis to be performed. All data sets were processed with a "collision detection filter" to univocally assign each IS to a patient and to one or more T cell subpopulations by applying a 10-fold rule for contamination identification as previously reported. Additional specifications are reported in the Methods section
Data analysis	Immunophenotyping: Raw data was analysed using FlowJo 10.6.2 (TreeStar). Graphical representations of Lymphocyte counts and IS analyses were generated with Prism8 (GraphPad Software). IS analyses were performed using R version 3.6.1 (packages used BiodiversityR, packcircles, hclust, Rcapture, gplots, corrplot, Mcorr) and Circos (http://circos.ca). Additional information is reported in the Methods section.

For manuscripts utilizing custom algorithms or software that are central to the research but not yet described in published literature, software must be made available to editors and reviewers. We strongly encourage code deposition in a community repository (e.g. GitHub). See the Nature Research guidelines for submitting code & software for further information.

Data

Policy information about availability of data

All manuscripts must include a data availability statement. This statement should provide the following information, where applicable:

- Accession codes, unique identifiers, or web links for publicly available datasets
- A list of figures that have associated raw data
- A description of any restrictions on data availability

The fastq files relative to sequencing of IS amplicons generated for this study are available through the NCBI repository (https://submit.ncbi.nlm.nih.gov/) BioProject ID PRJNA718947 and accession number generation is underway. Source data for Fig.1,2,4-8 and Extended Data Fig. 1,2,5-7 have been provided as Source Data files. All other data supporting the findings of this study are available from the corresponding author on reasonable request.

Field-specific reporting

Please select the one below that is the best fit for your research. If you are not sure, read the appropriate sections before making your selection.

☒ Life sciences ☐ Behavioural & social sciences ☐ Ecological, evolutionary & environmental sciences

For a reference copy of the document with all sections, see nature.com/documents/nr-reporting-summary-flat.pdf

Life sciences study design

All studies must disclose on these points even when the disclosure is negative.

Sample size	Sample size was constrained by limited clinical sample availability.
Data exclusions	All available healthy donors' and patients' samples are reported in the manuscript. Technically validated results were always included to the analyses and we did not apply any exclusion criteria for outliers.
Replication	For phenotypic characterization of T cells, Rainbow beads (RB) calibration was performed during the set up of the instrumentation for FACS analyses. RB acquisition was performed before each sample acquisition in order to achieve reproducible instrument setting among different experiments. All attempts at replication were successful. For VCN evaluation, qPCR was validated for reproducibility. We run each sample in triplicate and values are reported as mean of the three triplicates. All attempts at replication were successful. IS collection and analysis was conducted on a single experiment basis using a well established protocol. No attempt at replication has been necessary.
Randomization	The experimental design did not include allocation of samples to randomised experimental group.
Blinding	The experimental design did not include allocation to groups nor to blinding. There was no expected results prior to perform these analyses, therefore blinding tests were not applicable.

Reporting for specific materials, systems and methods

We require information from authors about some types of materials, experimental systems and methods used in many studies. Here, indicate whether each material, system or method listed is relevant to your study. If you are not sure if a list item applies to your research, read the appropriate section before selecting a response.

Materials & experimental systems

n/a	Involved in the study
☐	☒ Antibodies
☒	☐ Eukaryotic cell lines
☒	☐ Palaeontology and archaeology
☒	☐ Animals and other organisms
☐	☒ Human research participants
☐	☒ Clinical data
☒	☐ Dual use research of concern

Methods

n/a	Involved in the study
☒	☐ ChIP-seq
☐	☒ Flow cytometry
☒	☐ MRI-based neuroimaging

Antibodies

Antibodies used	CD19 CAT19 B12RIgG2a Evitria followed by secondary staining with Anti rat IgG PE for CAR detection (Biolegend 405406, 0.5ul), CD3 APC-Cy7 (Biolegend 300426, 5ul), 7-AAD (BD 555816, 5ul), CD95 BV711 (BD 563132, 5ul), CD45RA v450 (BD 8053598, 2ul) and CD62L APC (Biolegend 304810, 3ul).

Validation	All antibodies have been validated by manufacturers. Biolegend antibodies validation details can be found here https://www.biolegend.com/en-us/reproducibility BD antibodies are validated testing them on a combination of primary cells, cell lines and/or transfectant cell models with relevant controls using multiple immunoassays to ensure biological accuracy. BD also perform multiplexing with additional antibodies to interrogate antibody staining in multiple cell populations (source: https://www.biocompare.com/Antibody-Manufacturing/355107-Antibody-Manufacturing-Perspectives-BD-Bioscience/).

Human research participants

Policy information about studies involving human research participants

Population characteristics	PPatient 4 is a 21-year-old man who had a combined bone marrow and CNS relapse 1 year post matched unrelated donor peripheral blood stem cell transplant and was treated with 106 CAR+ T cells/kg in 3rd CR (molecular MRD 2.6 x 10-5) on 23/11/16. He is currently well in molecular CR with detectable circulating CAR T cells 3.5 years post infusion. Patient 6 is an 11-year-old boy who had a combined bone marrow and CNS relapse 14 months after a matched unrelated donor BMT for ALL and relapsed again in the CSF with molecular disease in the bone marrow 7 months after 2nd BMT. He was treated with 106 CAR+ T cells/kg (molecular MRD 5 x 10-4) on 5/10/16 and remains well in molecular CR with detectable circulating CAR T cells 3.5 years post infusion. Patient 10 was a 10-year-old boy with an isolated bone marrow relapse 17 months after matched family donor BMT who was treated with 106 CAR+ T cells/kg in 3rd CR (molecular MRD 3 x 10-5) on 30/8/17 with molecular CR and excellent initial CAR T cell expansion at 1 month but CAR T cells were undetectable by flow and qPCR from 2 months post-infusion. He relapsed with CD19 disease 7 months post CAR T cell therapy and subsequently died of a fungal infection. Patient 17 is a 15-year-old boy with late isolated CNS relapse who relapsed again in the CNS despite cranial irradiation and was treated with 106 CAR+ T cells/kg in 3rd CR (molecular MRD 5 x 10-5 negative) on 25/7/18 with continuing molecular CR and excellent initial CAR T cell expansion at 1 month but CAR T cells were undetectable by flow and qPCR from 4 months. He was consolidated with a mismatched unrelated donor BMT and remains in CR 2 years post-transplant.
Recruitment	Written informed consent was obtained from patients or their parents/guardians prior to study entry.
Ethics oversight	The CARPALL study (NCT02443831) was approved by the UK Medicines and Healthcare Products Regulatory Agency (clinical trial authorization no. 20363/0361/001) and ethical approval (including the research in this manuscript) was obtained from the London West London & GTAC Research Ethics Committee (REC ref no. 16/LO/0283). Written informed consent was obtained from patients or their parents/guardians prior to study entry.

Note that full information on the approval of the study protocol must also be provided in the manuscript.

Clinical data

Policy information about clinical studies

All manuscripts should comply with the ICMJE guidelines for publication of clinical research and a completed CONSORT checklist must be included with all submissions.

Clinical trial registration	The CARPALL study (NCT02443831) was approved by the UK Medicines and Healthcare Products Regulatory Agency (clinical trial authorization no. 20363/0361/001)
Study protocol	See attached clinical protocol
Data collection	The CARPALL study (NCT02443831) was a multi-centre, non-randomised, open label study conducted in 3 UK hospitals (Great Ormond St Children's Hospital, University College London Hospital and the Royal Manchester Children's Hospital) with data collection by the University College London Cancer Trial Centre. Patients for cohort 1 were recruited between May 2016 and June 2018. Data was collected on the interventional phase of the protocol for 2 years post CAR T cell infusion on the long term follow up phase for a further 8 years.
Outcomes	These were carefully defined during the design of the trial based on input from clinicians in this field. The outcomes were based on clinical importance to look at the effect of IMP. The outcome measures were looked at by analysing patient data periodically throughout the duration of the trial, and if required would have been amended. Primary: 1. Toxicity following CD19CAR T-cell administration as evaluated by the incidence of grade3-5 toxicity causally related to the ATIMP (particularly severe cytokine release syndrome, neurotoxicity) occurring within 30 days of CAR T-cell infusion. 2. Biological efficacy of CD19CAR T-cells as evaluated by the proportion of patients achieving a molecular remission (assessed by IgH qPCR and/or Next Generation Sequencing (NGS)) or flow MRD negativity (assessed by flow cytometry) at 1 month post CD19CAR T-cell infusion and duration of this response. Secondary: 1. Proportion of patients who are in molecular remission (IGH qPCR/NGS) and/or are flow MRD negative (flow cytometry) without further therapy at 2 years 2. Persistence and frequency of circulating CD19CAR T-cells in the peripheral blood of recipients after adoptive transfer as assessed by flow cytometry and qPCR 3. Incidence and duration of hypogammaglobulinaemia 4. Relapse rate, Disease-Free Survival and Overall Survival at 1 and 2 years after immunotherapy with CD19CAR transduced T-cells.

Flow Cytometry

Plots

Confirm that:

☒ The axis labels state the marker and fluorochrome used (e.g. CD4-FITC).

☒ The axis scales are clearly visible. Include numbers along axes only for bottom left plot of group (a 'group' is an analysis of identical markers).

☒ All plots are contour plots with outliers or pseudocolor plots.

☒ A numerical value for number of cells or percentage (with statistics) is provided.

Methodology

Sample preparation	Immunophenotyping and cell sorting Cells were thawed in RPMI (10% FCS) pre-warmed with DNase 200 u/ml (also used TexMACS 5% human AB serum). Cells were then washed, counted and stained on ice in 100 ul PBS for every 5x10^6 cells. Then Fc block was applied for 20 mins and without washing, anti-idiotype was added for 30 mins. Then cells were washed and stained for 30 mins with secondary antibody mix containing: 7-AAD, CD3 APC-Cy7 (CD62L APC, CD45RA v450, CD95 BV711). Then cells were washed and resuspend in sort buffer (PBS (1%FBS) + 1mM EDTA), and then sorted using FASCAriaIII cells sorter. Raw FACS data was collected using DIVA software (BD Biosciences) and analysed with FlowJo (TreeStar).
Instrument	Sorting was done with FACS Aria. Immunophenotyping was done with BD FACSCanto (BD Biosciences) (after Rainbow bead calibration (Spherotech)).
Software	Raw FACS data was collected using DIVA software (BD Biosciences) and analysed with either FlowJo (TreeStar)
Cell population abundance	Where possible we measured purity of sorted cells and sorted cells reached a purity ranging between 92% and 99%. Due to the low amount of starting materials we run in parallel an healthy donor sample to check the efficiency and purity of our sorting by acquiring sorted subpopulations at the analyzer. Moreover, the double-sorting strategy allows an internal control of purity of our sorted populations.
Gating strategy	Briefly, after gating on singlets, we gated on Lymphocytes and then we used CD62L and CD45RA to identify DP precursors CD4/CD8+ CD3+CD45RA+CD62L+; Central memory (TCM) CD4/CD8+ CD3+CD45RA-CD62L+; and Effector memory (TEM) CD4/CD8+ CD3+CD45RA-CD62L- cells. We then used CD95 marker to identify Naïve T cells (TN) CD4/CD8+ CD3+CD45RA+CD62L+CD95- and T stem cell memory (TSCM) CD4/CD8+ CD3+CD45RA+CD62L+CD95+ with the DP precursor population.

☒ Tick this box to confirm that a figure exemplifying the gating strategy is provided in the Supplementary Information.